Synthetic Turbulence Methods for Leading Edge Noise Predictions

Fernando Gea-Aguilera[*], Xin Zhang[†], Xiaoxian Chen[‡], and James Gill[‡]
Faculty of Engineering and the Environment,
University of Southampton, Southampton, SO16 7QF, UK.

Thomas Nodé-Langlois[§]
Acoustics and Environment - Numerical Methods,
Airbus Operations S.A.S, 31060 Toulouse, France.

An advanced digital filter method to generate synthetic turbulence is presented for efficient two- and three-dimensional leading edge noise predictions. The technique, which is based on the Random Particle-Mesh method, produces a turbulent inflow that matches a target isotropic energy spectrum. The discretized equations for the synthetic eddies, and the input parameters needed to recover the desired turbulence statistics, are presented. Moreover, a simple and fast implementation strategy, which does not require an additional boundary condition, is presented under the frozen turbulence assumption. The method is used in a linearized Euler solver to predict turbulence-airfoil interaction noise from a number of configurations, including variations in airfoil thickness, angle of attack and Mach number. For the first time, noise predictions from a digital filter method are directly compared to those provided by synthetic turbulence based on a summation of Fourier modes. The comparison indicates that the advanced digital filter method gives enhanced performance in terms of computational cost and simulation accuracy. In addition, initial tests show that this method is capable of reproducing experimental noise measurements within 3 dB accuracy.

Keywords: computational aeroacoustics, synthetic turbulence, digital filter, leading edge noise

I. Introduction

Over the past few decades, commercial aviation has experienced a large increase in the number of passengers and goods transported. This expansion has been accompanied by a reduction in flight hours and fuel costs, which has helped to develop the economic globalization and emerging economies. Furthermore, air traffic is forecast to grow in the coming years.[1] In order to ensure a sustainable development, this growth must be associated with a reduction in the environmental impact of aviation.[2]

In the 60's, jet noise produced by turbojet-powered aircraft was the dominant source of noise, particularly due to the turbulent mixing between the jet and the external flow around the nacelle. Today, modern turbofan engines have significantly reduced jet noise by shielding the hot stream with a cold by-pass exhaust stream and by increasing the by-pass ratio. Thus, fan noise has become the biggest challenge when attempting to reduce engine noise at take-off and approach, whilst the influence of the compressor and turbine stages remains quieter than the fan.[3]

[*]PhD Student, Airbus Noise Technology Centre, AIAA Student Member, F.Gea-Aguilera@soton.ac.uk.
[†]Airbus Noise Technology Centre. Also Chair Professor, Department of Mechanical and Aerospace Engineering, The Hong Kong University of Science and Technology, Clear Water Bar, Kowloon, Hong Kong SAR, China. Associate Fellow, AIAA.
[‡]Research Fellow, Airbus Noise Technology Centre.
[§]Acoustic Engineer, Acoustics and Environment Department, Airbus.

Figure 1 shows a schematic representation of the main sources of engine fan broadband noise. Ganz *et al.*[4] ran a series of experiments to quantify the contribution of different noise sources to the engine fan broadband noise. According to their experiment, the rotor-stator wake interaction noise was found to be the greatest contributor. Leading edge noise, also known as turbulence-airfoil interaction noise, is important because it is the underlying cause of both turbulence ingestion noise and rotor-stator wake interaction noise. Furthermore, leading edge noise is not only relevant for turbofan engines but also for contra-rotating open-rotors and wind turbines. Therefore, a good understanding of the main factors that influence leading edge noise is required for effective noise prediction and reduction.

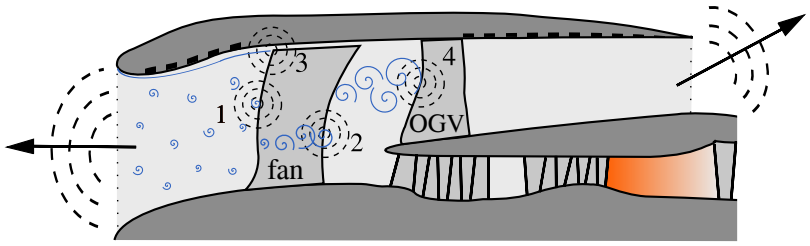

Figure 1. Fan broadband noise sources. Turbulence ingestion noise (1), fan and Outlet Guide Vane (OGV) trailing edge noise (2), boundary layer rotor tip interaction noise (3) and rotor-stator wake interaction noise (4). Both upstream (forward-arc) and downstream (rear-arc) radiated noise are also shown.

II. Aims and Content of the Current Work

By using a Computational AeroAcoustics (CAA) solver, the current work addresses the following topics:

- An advanced digital filter method, which is based on the Random Particle-Mesh (RPM) technique,[5,6] is introduced to realize two-dimensional and three-dimensional isotropic synthetic turbulence for CAA applications.
- Low-cost three-dimensional leading edge noise predictions are made from two-dimensional CAA simulations in order to reproduce experimental results.
- A direct comparison in terms of accuracy and computational cost is made between the advanced digital filter method presented in this paper and synthetic turbulence based on Fourier modes. Among them, a one-component Fourier mode method, which only models the transverse velocity disturbance, and a two-component Fourier mode method, which includes both streamwise and transverse components, are analyzed.
- Mach number, airfoil thickness and angle of attack effects on leading edge noise predictions from isolated airfoils are investigated for different synthetic turbulence methods. The suitability of the non-uniform mean flow assumption is also examined by means of turbulence spectra near the stagnation point.

The content is organized as follows. Section III presents a review on previous computational studies based on the combined use of the Linearized Euler Equations (LEEs) and synthetic turbulence for leading edge noise predictions. Then, the characteristics of the CAA solver used in this work are detailed in Section IV. The two-dimensional advanced digital filter method is presented and validated for leading edge noise predictions in Section V. This method is compared to those based on Fourier modes to perform turbulence-airfoil interaction noise simulations on a number of isolated airfoil configurations in Section VI. Finally, an extension of the advanced digital filter method to realize a fully three-dimensional turbulent field is presented and validated in Section VII.

III. Previous Work

Current limitations of analytical models to predict leading edge noise from airfoils with real geometry, and the difficulty of isolating the source of noise under study in experiments, make numerical simulations an interesting alternative for broadband noise predictions. Although Direct Numerical Simulation (DNS)

can be used for acoustic simulations, the associated cost is currently prohibitive in an industrial context, where high Reynolds numbers are often required.[7] In addition, other sources of noise, such as trailing edge noise, would be present in the simulation. Alternative approaches, retaining at least the main features of the physical problem, have already been considered. To this end, leading edge noise simulations from isolated airfoils are performed by means of different CAA methods. Typically, these use either linearized or full Euler equations to simulate the noise generation and propagation. Since the viscous terms are neglected, synthetic turbulence with the desired statistical properties has to be prescribed for its interaction with the airfoil.

Early works in this field focused on gust-airfoil interaction noise simulations. In particular, transverse and skewed harmonic gusts were used to show the effects on the noise directivity due to airfoil thickness and angle of attack (for instance, see Atassi *et al.*,[8] Lockard and Morris[9]). Gill *et al.*[10] used a multi-frequency gust approach in which several harmonic gusts were employed to study the effect of airfoil thickness.

Synthetic turbulence based on a summation of Fourier modes can be obtained by superimposing a number of harmonic gusts, whose amplitude is proportional to the square root of an energy or velocity spectrum. The use of Fourier modes to generate stochastic turbulent fields was first proposed by Kraichnan,[11] when studying the scalar diffusion of fluid particles. These methods have been extensively used for CAA applications, such as subsonic jet noise,[12,13] due to their simple implementation and their ability to reproduce a target turbulence spectrum.

In the area of leading edge noise predictions, Clair *et al.*[14] used a one-component Fourier mode approach to calculate the noise radiated by a three-dimensional airfoil with reduced span in a LEE code. This type of turbulent inflow is based on the analytical model by Amiet,[15] who showed that the transverse unsteady velocity is responsible for the broadband noise radiated by a flat plate at zero incidence.

Further investigation on the number of fluctuating velocity components that is required to address leading edge noise predictions using Fourier modes was performed by Gill.[16] The transverse fluctuating velocity plays a non-negligible role on the noise generation, whereas the chordwise and spanwise velocity disturbances have minor effects for symmetric airfoils at zero angle of attack. This finding may help to reduce the number of components to be used in CAA simulations and, therefore, decrease the computational expense.

Apart from methods based on Fourier modes, digital filter techniques were also proposed for turbulence synthesis in CAA applications. In this sense, the RPM method due to Ewert[5] was used to study airframe noise[5] and trailing edge noise.[17] In this family of methods, velocity fluctuations are defined by taking the curl of the vector potential, which ensures the divergence-free condition. Although the RPM method was originally developed to realize Gaussian energy spectra, Siefert and Ewert[18] showed that non-Gaussian energy spectra can also be obtained through a superposition of Gaussian spectra.

Following Ewert's work,[5] Dieste and Gabard[6] derived the exact expressions for the filters that can realize two-dimensional Liepmann and von Kármán isotropic energy spectra. These were tested on leading edge noise simulations of a flat plate. The synthetic turbulence was calculated on the flat plate surface and imposed through a wall boundary condition in a LEE solver for the noise propagation. Such an implementation cannot account for the distortion of the turbulence structures around thick airfoils in non-uniform mean flows.

To overcome this limitation, Wohlbrandt *et al.*[19] tested a number of numerical implementations to adapt the RPM method for leading edge noise predictions. Among them, a combined approach between the Acoustic Perturbation Equations[20] (APEs) and the LEEs, and a buffer zone coupled with the LEEs were proposed.

In order to reduce the number of grid points where the velocity fluctuations have to be calculated when using a buffer zone, Kim *et al.*[21] proposed two types of inflow boundary condition for a RPM-based method to be used in LEE solvers. One of them follows Tam *et al.*'s radiation boundary condition.[22] The other one is based on the characteristic waves of the Euler equations proposed by Giles.[23] This technique was used in a recent work to study noise reduction due to thick airfoil in inviscid mean flows.[24]

Synthetic eddy methods, which were initially developed for LES applications,[25,26] have also been proposed for leading edge noise predictions. In this sense, Kim and Haeri[27] investigated the effect of wavy leading edges on flat plates through a set of three-dimensional simulations using the full Euler equations. The target energy spectrum is realized through a superposition of synthetic eddies under certain constraints. The stochastic turbulence is introduced through a buffer zone at the edge of the computational domain and convected by the mean flow as frozen turbulence.

IV. CAA Method

The present work uses a high-order finite difference CAA solver, called SotonCAA, that has been developed within the University of Southampton and used in prior CAA studies.[28,29,30]

In this study, the LEEs are solved in the time-domain by using a 4th-order implicit spatial scheme.[31] The numerical solution is filtered after each time-step in order to assure the numerical stability of the simulation. To this end, a compact filter with variable cut-off wavenumber[32] is employed along with a 4-6 Low Dispersion and Dissipation Runge-Kutta (LDDRK) scheme.[33]

A slip-wall boundary condition is used on the airfoil surface. Additionally, implicit buffer zones[34] are applied in order to prevent sound waves from being reflected at the edge of the CAA domain.

Numerical simulations presented in this work were run with mean flow density $\rho_0 = 1.2\,\mathrm{Kg/m^3}$ and speed of sound $c_0 = 340\,\mathrm{m/s}$, unless otherwise stated. The reference speed is $U_{ref} = 1\,\mathrm{m/s}$. The reference values for the Sound Pressure Level (SPL) and sound PoWer Level (PWL) calculations are $2 \times 10^{-5}\,\mathrm{N/m^2}$ and $1 \times 10^{-12}\,\mathrm{W}$, respectively.

All computations used the IRIDIS high performance computing facility at the University of Southampton.

V. Two-dimensional Advanced Digital Filter Method

An advanced digital filter method for efficient leading edge noise predictions is proposed in this section. The technique developed herein relates the energy spectrum to a summation of Gaussian spatial filters in order to match the desired isotropic energy spectrum.

The method is presented for a purely two-dimensional turbulent inflow in Section V.A. Although two-dimensional turbulence was used in a number of works,[6,24] it cannot be employed to reproduce experimental results without applying some correction factors.[17] This is due to the fact that the governing equations for two-dimensional isotropic velocity spectra differ from those of three-dimensional turbulence. To overcome this problem while keeping a reduced computational cost, the method is extended to realize a two-dimensional slice of three-dimensional turbulence under the $k_z = 0$ assumption in Section V.B. This assumption follows Amiet's work,[15] in which the spanwise wavenumber (k_z with the notation used in this work) does not contribute to the far-field acoustic power for observers at the mid-span plane if the span is much larger than the turbulent integral length scale.

Although Dieste and Gabard[6] developed analytical expressions for the von Kármán and Liepmann filters under the assumption of two-dimensional isotropic turbulence, a superposition of Gaussian spectra is used herein. This option is preferred since the equations of the filters for the non-Gaussian spectra go beyond the simplicity of the exponential function that defines a Gaussian filter. In addition, it requires the derivation of a new set of governing equations for each type of energy spectrum to be matched, which is a less generic option.

Taylor's frozen[35] turbulence was found to be suitable for broadband noise predictions when compared to evolving turbulence, i.e., when the time decorrelation is included in the analysis.[6] In this work, frozen turbulence is considered for the turbulent inflow since the vortical disturbances are introduced into the CAA domain upstream of the airfoil and are convected by the mean flow. This allows the vortical wavenumber to be linked to the acoustic frequency by $2\pi f = \mathbf{k} \cdot \mathbf{U}$, where f is the frequency, $\mathbf{k}$ is the wave vector and $\mathbf{U}$ is the mean flow velocity.

V.A. Two-dimensional Turbulence

After discretization of the RPM governing equations, the resulting turbulent flow is obtained from a summation of fluctuating velocity fields due to small particles. Each particle acts as an eddy, which introduces a divergence-free velocity field around its center and vanishes far from it. In the current digital filter formulation, all eddies have the same amplitude and the only difference between them is the direction of rotation. Thus, no white-noise signal has to be filtered, which speeds up the simulations and highlights similarities between the current implementation and synthetic eddy methods. Since frozen turbulence is assumed, the eddies can be introduced into the CAA domain through an inlet section without using an additional boundary condition[6,19,21] (see Figure 2). This synthetic turbulence method is presented in Section V.A.1 and validated for leading edge noise predictions in Section V.A.2.

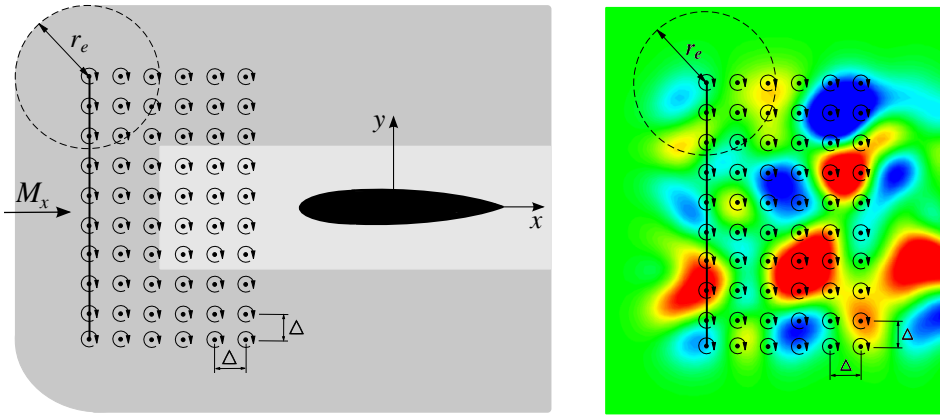

Figure 2. Synthetic eddies and inlet section parameters (r_e and Δ). Light gray background represents the region where the desired statistical properties are obtained.

V.A.1. Non-Gaussian Energy Spectra Through Gaussian Superposition

Following a Lagrangian formulation,[6] the two-dimensional turbulent field can be written as the contribution of p small particles that define the whole source region $V_s = \sum_{p=1}^{p=P} V_{s,p}$. It reads

$$u_x(\mathbf{x},t) = \sum_{p=1}^{P} \frac{\partial}{\partial y} G(\mathbf{x}-\mathbf{x}_e)\mathcal{U}_p, \tag{1}$$

$$u_y(\mathbf{x},t) = -\sum_{p=1}^{P} \frac{\partial}{\partial x} G(\mathbf{x}-\mathbf{x}_e)\mathcal{U}_p, \tag{2}$$

where $G(\mathbf{x}-\mathbf{x}_e)$ is the spatial filter, $\mathbf{x}$ is a point in the flow field, $\mathbf{x}_e$ is the center of each small element and $\mathcal{U}_p$ represents the white-noise term averaged over each small element $V_{s,p}$,

$$\mathcal{U}_p = \int_{V_{s,p}} \mathcal{U}(\mathbf{x}',t)\mathrm{d}\mathbf{x}'. \tag{3}$$

Using the white-noise properties for frozen turbulence,[5] it is possible to show that the mean value of the white noise term is $\langle \mathcal{U}_p \rangle = 0$, and its variance follows $\langle \mathcal{U}_p^2 \rangle = \Delta^2$, where $\langle . \rangle$ is the ensemble average operator and Δ is the distance between the eddy centers, as shown in Figure 2. Therefore, $\mathcal{U}_p$ can be obtained from a normal distribution $\mathcal{N}(0,\Delta)$. This allows the velocity field introduced by each eddy to be rewritten as,

$$u_x(\mathbf{x}) = +\epsilon\Delta \frac{\partial}{\partial y} G(\mathbf{r}), \tag{4}$$

$$u_y(\mathbf{x}) = -\epsilon\Delta \frac{\partial}{\partial x} G(\mathbf{r}), \tag{5}$$

where $\mathbf{r} = \mathbf{x}-\mathbf{x_e}$, and ϵ randomly takes the values $+1$ or -1, which makes it satisfy $\langle \epsilon \rangle = 0$. In this derivation, the white-noise term usually found in RPM methods is replaced by $\epsilon\Delta$, which speeds up the simulations and the convergence of the velocity spectra. This novel and efficient implementation also highlights similarities between RPM and synthetic eddy methods. Thus, ϵ can be seen as a parameter that defines the direction of rotation for each eddy and Δ controls the amplitude of the eddies depending on the number of vortices that are introduced through the inlet section.

The isotropic energy spectrum is linked to the spatial filter in wavenumber space[6] by

$$E^{2\mathrm{D}}(k) = 4\pi^3 k^3 \hat{G}(k)^2, \tag{6}$$

where k is the overall wavenumber and the Fourier transform[a] of the spatial filter is defined as,

$$\hat{G}(k) = \frac{1}{4\pi^2} \int_{-\infty}^{+\infty} G(\mathbf{r}) \exp\left[-i\mathbf{k}\cdot\mathbf{r}\right] \mathrm{d}\mathbf{r}. \tag{7}$$

[a]The convention for the Fourier transform adopted in this work is the same as in Pope.[36]

Since the desired energy spectrum can be obtained from a superposition of Gaussian spectra, the equations of the fluctuating velocity are first derived according to Kraichnan's[11] Gaussian spectrum,

$$E^{2D}(k) = \frac{2}{\pi^2} u_{rms}^2 \Lambda^4 k^3 \exp\left(-\frac{\Lambda^2 k^2}{\pi}\right), \tag{8}$$

where u_{rms} is the root-mean-square of the turbulent velocity and Λ is the integral length scale. Introducing Eq. 8 into Eq. 6 and performing the inverse Fourier transform, the Gaussian filter in physical space takes the form,

$$G(r) = \sqrt{\frac{2u_{rms}^2}{\pi}} \exp\left(-\frac{\pi r^2}{2\Lambda^2}\right). \tag{9}$$

Therefore, the two-dimensional fluctuating velocity field due to a single eddy can be expressed as

$$u_x(\mathbf{x}) = -\frac{\epsilon\Delta}{\Lambda^2}\sqrt{2\pi u_{rms}^2}\,(y - y_e)\exp\left(-\frac{\pi r^2}{2\Lambda^2}\right), \tag{10}$$

$$u_y(\mathbf{x}) = +\frac{\epsilon\Delta}{\Lambda^2}\sqrt{2\pi u_{rms}^2}\,(x - x_e)\exp\left(-\frac{\pi r^2}{2\Lambda^2}\right). \tag{11}$$

Figure 3 shows velocity contours and normalized velocity magnitude (cross-section) of a two-dimensional Gaussian eddy according to Eqs. 10 and 11.

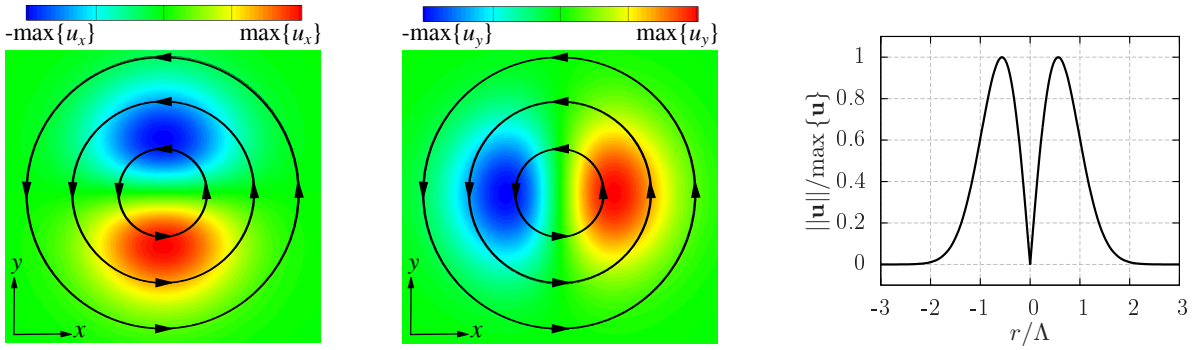

(a) u_x contours and streamlines. (b) u_y contours and streamlines. (c) Eddy cross-section.

Figure 3. Fluctuating velocity field due to a two-dimensional Gaussian eddy.

As shown in Figure 2, the ability of the synthetic turbulence to realize the desired statistical properties relies on two parameters: the distance between the eddy centers, Δ, and the radius of the eddies, r_e. Dieste[37] suggested for Gaussian spectra $r_e = 2.43\Lambda$ and $\Delta = \Lambda/6$. In the present work, it is shown that these values can be reduced without affecting the quality of the synthetic turbulence. In particular, provided that $r_e \geq 3\Lambda/2$ and $\Delta \leq \Lambda/2$, the target turbulence statistics are recovered. These new limiting values allow to decrease the size and the number of eddies to be injected through the inlet section, which reduces the amount of grid points where the synthetic turbulence has to be evaluated.

Validation cases were run in a computational domain with uniform grid spacing and mean flow speed $U_x = 60\,\mathrm{m/s}$. The integral length scale and the turbulence intensity are $\Lambda = 0.008\,\mathrm{m}$ and $T_u = u_{rms}/U_x = 0.017$, respectively. The quality of the synthetic turbulence was assessed by calculating one-dimensional spectra defined as,[36]

$$E_{11}^{2D}(k_x) = 2\int_{-\infty}^{+\infty} \Phi_{11}^{2D}(k_x, k_y)\mathrm{d}k_y, \tag{12}$$

$$E_{22}^{2D}(k_x) = 2\int_{-\infty}^{+\infty} \Phi_{22}^{2D}(k_x, k_y)\mathrm{d}k_y, \tag{13}$$

where $\Phi_{11}^{2D}(k_x, k_y)$ and $\Phi_{22}^{2D}(k_x, k_y)$ are the velocity spectra of the streamwise and the transverse fluctuating velocity, respectively. These are obtained from the Fourier transform of the two-point velocity correlation, which can be calculated from independent velocity samples.

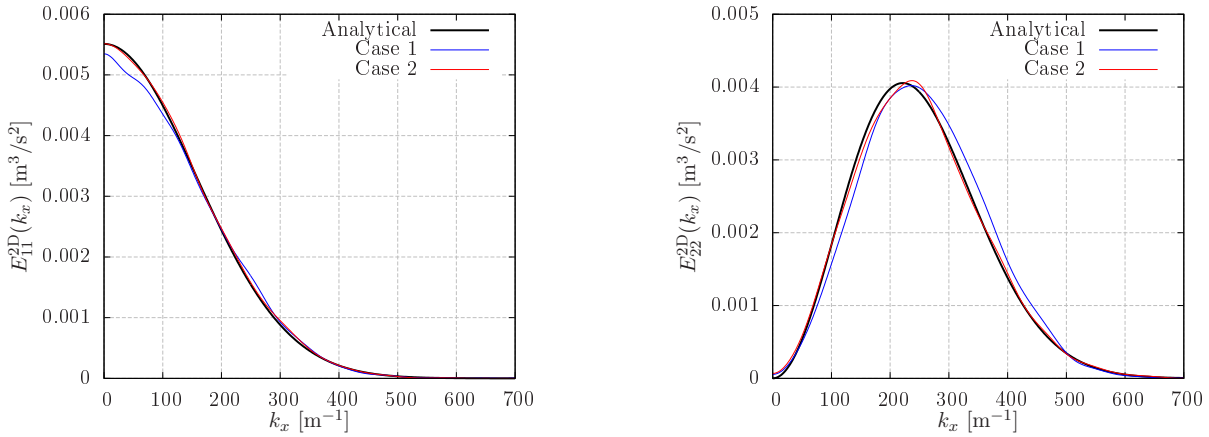

(a) E_{11}^{2D}. (b) E_{22}^{2D}.

Figure 4. One-dimensional Gaussian spectra (12,000 samples). Case 1 corresponds to $\Delta = \Lambda/2$ and $r_e = 3\Lambda/2$ and Case 2 corresponds to $\Delta = \Lambda/6$ and $r_e = 5\Lambda/2$.

Figure 4 shows analytical and numerical one-dimensional spectra for the two combinations of parameters under study. In both cases, numerical results closely match the analytical expressions. Despite of a noticeable difference in the r_e and Δ values, the difference in computational time is less than 5% for the validation cases presented in this section. This is due to the implementation strategy, which identifies the grid points in the computational domain that are affected by the inlet section and pre-evaluates the amplitude of the eddies acting on each grid point at the very beginning of the simulation. This means that a significant increase in r_e or Δ has little effect on the computational time, at least for two-dimensional CAA domains.

It should also be noted that although each eddy is divergence-free by definition, some spurious noise may appear around the inlet section as the eddies are superimposed on the mean flow velocity. This spurious noise depends on the grid quality, r_e and Δ. If the grid is not fine enough to smoothly reproduce the shape of the eddies or the eddies are truncated at a value close to $r_e = 3\Lambda/2$, background noise is expected to be relatively high around the inlet section. The first is related to the number of points per wavelength that is required for the solver to convect the eddy by the mean flow. For instance, in validation *Case 1*, eleven grid points were used along the radius of the eddy. The second is due to the fact that at $r_e = 3\Lambda/2$ the normalized amplitude of the eddy is $\|\mathbf{u}\|/\max\{\mathbf{u}\} = 0.128$, as shown in Figure 3(c). At that location the derivatives $\partial u_x/\partial x$ and $\partial u_y/\partial y$ are not close to zero, which leads to a local break down of the divergence-free condition. Nevertheless, the amplitude of these spurious pressure fluctuations is of the order of 10^3 times smaller than those due to the turbulence-airfoil interaction in all simulations presented in Section VI. Thus, its influence in the leading edge noise predictions can be neglected and the turbulence does not need to be injected through a buffer zone.

An extension of the previous Gaussian digital filter method is developed in order to match a desired energy spectrum within the wavenumber range under study. The main idea is to define a new eddy shape as a superposition of several Gaussian eddies, each of them with a different integral length scale, Λ_i, and turbulent kinetic energy, $u_{rms,i}^2$.

It is possible to define a digital filter as a summation of N_e Gaussian filters in wavenumber space,

$$\hat{G}_{sum}(k) = \sum_{i=1}^{N_e} \hat{G}_i(\Lambda_i, u_{rms,i}^2, k), \tag{14}$$

where, according to Eqs. 6 and 8, each filter reads

$$\hat{G}_i(\Lambda_i, u_{rms,i}^2, k) = \frac{\Lambda_i^2}{\pi^2}\sqrt{\frac{u_{rms,i}^2}{2\pi}}\exp\left(-\frac{\Lambda_i^2 k^2}{2\pi}\right). \tag{15}$$

Using Eq. 6, the target energy spectrum (e.g. von Kármán, Liepmann, etc.) can be approximated by

$$E_{sum}^{2D}(k) = 4\pi^3 k^3 \left[\sum_{i=1}^{N_e} \hat{G}_i(\Lambda_i, u_{rms,i}^2, k)\right]^2. \tag{16}$$

Introducing Eq. 15 into Eq. 16, straightforward algebra shows that

$$E_{sum}^{2D}(k) = \frac{2k^3}{\pi^2} \sum_{i=1}^{N_e}\sum_{j=1}^{N_e} \sqrt{u_{rms,i}^2 u_{rms,j}^2}\,(\Lambda_i\Lambda_j)^2 \exp\left[-\frac{k^2}{2\pi}\left(\Lambda_i^2+\Lambda_j^2\right)\right], \tag{17}$$

or equivalently,

$$E_{sum}^{2D}(k) = \frac{2k^3}{\pi^2}\left\{\sum_{i=1}^{N_e} u_{rms,i}^2 \Lambda_i^4 \exp\left(-\frac{k^2\Lambda_i^2}{\pi}\right) + \sum_{i=1,i\neq j}^{N_e}\sum_{j=1}^{N_e} \sqrt{u_{rms,i}^2 u_{rms,j}^2}\,(\Lambda_i\Lambda_j)^2 \exp\left[-\frac{k^2}{2\pi}\left(\Lambda_i^2+\Lambda_j^2\right)\right]\right\}. \tag{18}$$

From Eq. 17, it follows that the resulting energy spectrum from the superposition process only matches the target energy spectrum within the wavenumber range of interest. Therefore, the total turbulent kinetic energy of the target energy spectrum is not completely recovered. In addition, it is clear that the resulting energy spectrum is not just a summation over the Gaussian energy spectra, which corresponds to the first term on the right hand side in Eq. 18. The resulting velocity field introduced by each eddy from the Gaussian superposition reads,

$$u_x(\mathbf{x}) = -\epsilon\Delta \sum_{i=1}^{N_e} \frac{\sqrt{2\pi u_{rms,i}^2}}{\Lambda_i^2}(y-y_e)\exp\left(-\frac{\pi r^2}{2\Lambda_i^2}\right), \tag{19}$$

$$u_y(\mathbf{x}) = +\epsilon\Delta \sum_{i=1}^{N_e} \frac{\sqrt{2\pi u_{rms,i}^2}}{\Lambda_i^2}(x-x_e)\exp\left(-\frac{\pi r^2}{2\Lambda_i^2}\right). \tag{20}$$

An appropriate set of parameters N_e , Λ_i and $u_{rms,i}^2$ is required to reproduce the shape of the desired energy spectrum. Although there is not a unique combination of parameters for a given energy spectrum, proposed values from an optimization subroutine are given for most simulations presented in this work when using the advanced digital filter method.

In order to validate this Gaussian superposition technique, the method is applied to reproduce the two-dimensional von Kármán energy spectrum, which is defined as

$$E^{2D}(k) = \frac{110 u_{rms}^2 \Lambda}{27\pi} \frac{\left(\frac{k}{k_e}\right)^4}{\left[1+\left(\frac{k}{k_e}\right)^2\right]^{17/6}}, \tag{21}$$

where $k_e = \left[\sqrt{\pi}\Gamma(5/6)\right]/\left[\Lambda\Gamma(1/3)\right]$ with $\Gamma()$ as the Gamma function.

In this case, an accurate representation of the energy spectrum is obtained by using $N_e = 5$ different Gaussian eddies[b], whose integral length scale and the amplitude of the eddies are given in Table 1. These values are optimized to realize the two-dimensional von Kármán spectrum with $\Lambda = 0.008\,\mathrm{m}$ and $T_u = 0.017$. The mean flow speed was set to $U_x = 60\,\mathrm{m/s}$. Since the new eddies are obtained from a combination of several Gaussian eddies, limiting values to realize non-Gaussian energy spectra are based on the largest and smallest Gaussian eddies involved. Thus, $\Delta \leq \min\{\Lambda_i\}/2$ and $r_e \geq 3\max\{\Lambda_i\}/2$. These limiting values are validated through a comparison of numerical and analytical one-dimensional spectra, as shown in Figure 5.

Λ_i [m]	$u_{rms,i}^2$ [m^2/s^2]
2.524×10^{-2}	1.805×10^{-2}
1.401×10^{-2}	7.478×10^{-2}
7.285×10^{-3}	1.046×10^{-1}
3.023×10^{-3}	1.622×10^{-1}
2.238×10^{-3}	3.098×10^{-3}

Table 1. Parameters for validation of Gaussian superposition technique.

[b]In practical cases such as those presented in Section VI, N_e ranges between 4 and 6.

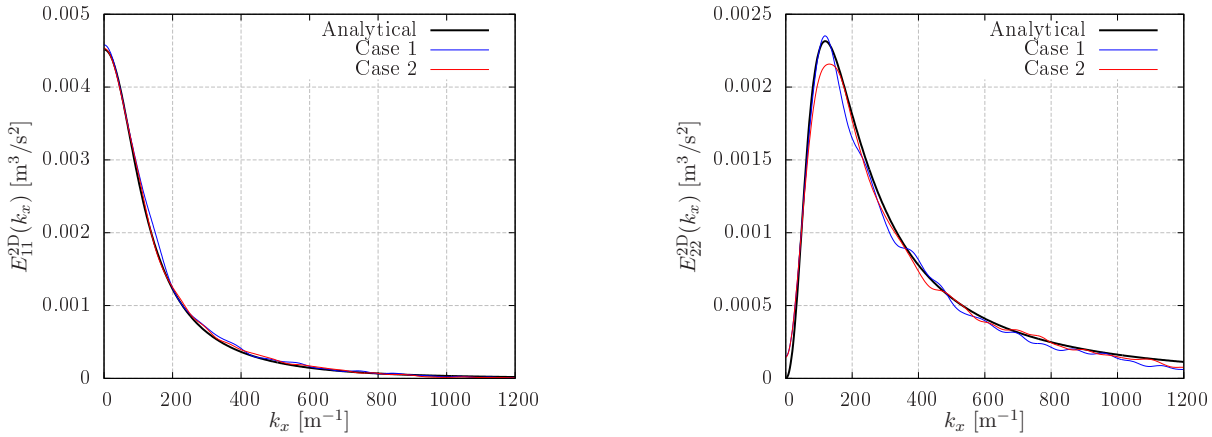

(a) E_{11}^{2D}. (b) E_{22}^{2D}.

Figure 5. One-dimensional von Kármán spectra through Gaussian superposition (12,000 samples). Case 1 corresponds to $\Delta = \min\{\Lambda_i\}/2$ and $r_e = 3\max\{\Lambda_i\}/2$ and Case 2 corresponds to $\Delta = \min\{\Lambda_i\}/6$ and $r_e = 5\max\{\Lambda_i\}/2$.

V.A.2. Validation Case: Two-dimensional NACA 0001 Airfoil

The advanced digital filter method is now validated for leading edge noise predictions from isolated airfoils. A NACA 0001 airfoil with chord $c = 0.15\,\text{m}$ at $M_x = 0.6$ is chosen. Results are compared with the flat plate analytical model developed by Amiet,[15] and adapted by Blandeau *et al.*[38] for two-dimensional noise radiation. As in the analytical model, the background mean flow is assumed to be uniform in the CAA domain.

Figure 6 shows the reference frame that is considered in this work for two-dimensional configurations. The size of the CAA domain extends to four times the chord in all directions around the airfoil mid-chord.

In this validation case, $N_e = 5$ is set in order to match the von Kármán energy spectrum with $\Lambda = 0.008\,\text{m}$ and $T_u = 0.017$. The values of their amplitude and integral length scale are shown in Table 2. These are employed to calculate the distance between eddies and the eddy radius, which are set to $\Delta = \min\{\Lambda_i\}/6$ and $r_e = 5\max\{\Lambda_i\}/2$, respectively. Since the mean flow is uniform, the inlet section can be placed at r_e upstream of the airfoil leading edge.

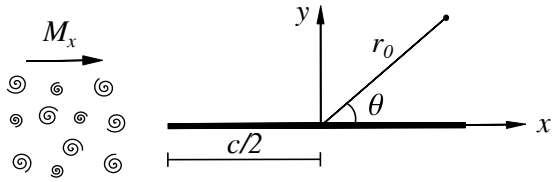

Figure 6. Two-dimensional flat plate configuration, where M_x is the mean flow Mach number, c is the airfoil chord, and the far-field observer position is defined by r_0 and θ.

The time step is set to $1.18 \times 10^{-8}\,\text{s}$ and the simulation is run for 8.625×10^6 time steps. The transitory state of the simulation lasts until the first set of eddies introduced within the CAA domain is convected past the airfoil. This represents about 1.5% of the simulation time.

In order to assess the quality of the turbulent inflow, a monitor point is placed upstream of the airfoil leading edge, where samples of velocity disturbances are collected every 283 time steps. These are used to calculate one-dimensional spectra[c], as illustrated in Figure 7. The advanced digital filter method shows an agreement within 1.5 dB for the majority of the frequency range in comparison with the analytical expressions. Although the agreement is satisfactory, a better match is possible if the simulation is run for longer.

Λ_i [m]	$u_{rms,i}^2$ [m^2/s^2]
2.524×10^{-2}	2.077×10^{-1}
1.401×10^{-2}	8.608×10^{-1}
7.285×10^{-3}	1.205
3.023×10^{-3}	1.867
2.238×10^{-3}	3.566×10^{-2}

Table 2. Parameters for Gaussian superposition in validation case of a NACA 0001 airfoil interacting with purely two-dimensional turbulence.

A second-order accurate Ffowcs-Williams and Hawkings (FW-H) solver, which is based on Farassat and Succi formulation 1A,[39] is used to predict the far-field noise. This solver assumes a uniform mean flow outside the collection surface, which is placed on the airfoil surface. This is consistent with the assumption of uniform mean flow in the CAA simulation of the NACA 0001 airfoil.

[c]When frozen turbulence is assumed, $E_{11}(f) = 2\pi E_{11}(k_x)/U_x$ and $E_{22}(f) = 2\pi E_{22}(k_x)/U_x$.

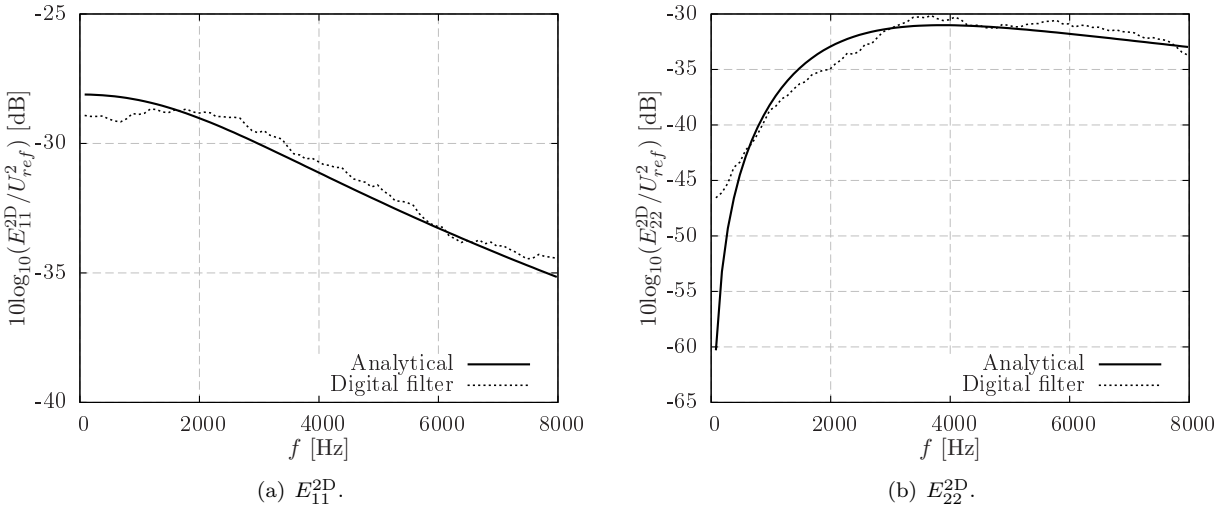

(a) E_{11}^{2D}. (b) E_{22}^{2D}.

Figure 7. E_{11}^{2D} and E_{22}^{2D} spectra for two-dimensional NACA 0001 airfoil in a uniform mean flow with $M_x = 0.6$ at approximately $0.02c$ upstream of the airfoil leading edge.

All observers are placed at $r_0 = 100c$ from the airfoil mid-chord, ranging from $\theta = 0^o$ to $\theta = 360^o$ every $\Delta\theta = 1^o$.

Figure 8(a) shows spectra of PWL per unit span and SPL. The advanced digital filter method provides noise predictions within 1.5 dB accuracy for the majority of the frequency range under study, which is clearly related to the convergence of the velocity spectra. For instance, Figure 7(b) shows an under-prediction of about 1.5 dB at 2000 Hz in the transverse one-dimensional spectrum, which is directly reflected on the PWL spectrum.

Directivity plots are also affected by the convergence of the velocity spectra. This is shown in Figure 8(b), where the advanced digital filter method under-predicts the SPL by about 1.5 dB at all observer positions. Nevertheless, the method is able to reproduce the right position of the lobes due to the loss of compactness at high-frequencies.

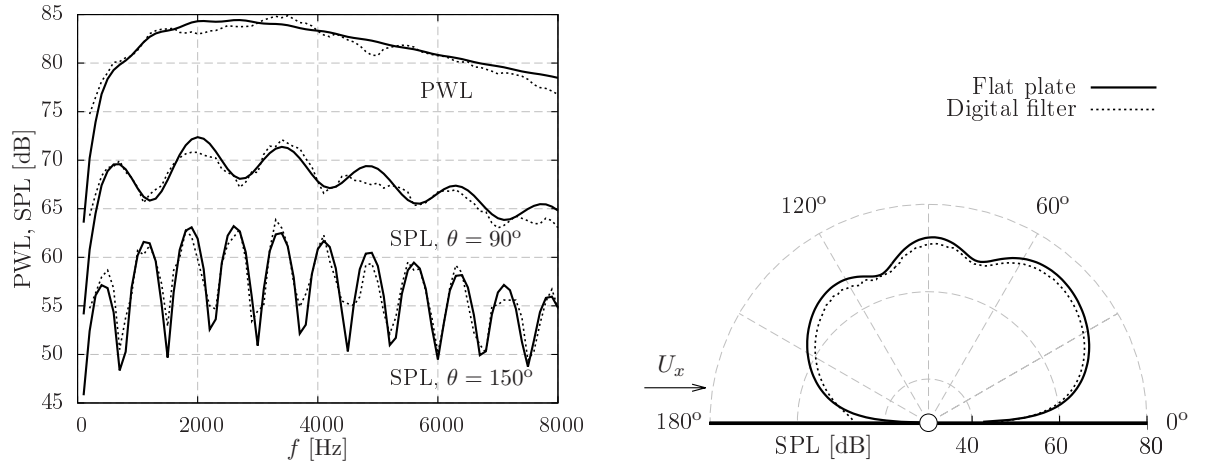

(a) PWL and SPL spectra. (b) Directivity pattern at $f = 2000$ Hz.

Figure 8. Far-field noise predictions from a two-dimensional NACA 0001 airfoil at $r_0 = 100c$.

V.B. Pseudo Three-dimensional Turbulence

Noise predictions from numerical simulations using purely two-dimensional turbulence cannot be directly compared with experimental results. A turbulence spectrum correction needs to be applied to account for

the shape of the three-dimensional velocity spectra. Additionally, the acoustic power decays as $1/r_0^2$ in a three-dimensional free field, whereas it decays as $1/r_0$ in case of a two-dimensional free field.

In this section, a technique to realize a divergence-free two-dimensional turbulent field that follows the governing equations of three-dimensional turbulence under the hypothesis of $k_z = 0$ is presented. This avoids the need of correction factors used in other works.[17] This type of turbulence is referred to as 'pseudo three-dimensional turbulence' in this work.

According to Amiet's theory,[15] the spanwise wavenumber does not contribute to the far-field acoustic power for observers at the mid-span plane if the span is much larger than the turbulent integral length scale. This assumption was employed by authors such as Clair *et al.*[14] and Gill[16] when using synthetic turbulence based on Fourier modes. In these methods the amplitude of each mode is proportional to the square root of the velocity or energy spectrum, which makes it straightforward to set $k_z = 0$. The same assumption can also be made when using digital filter methods.

For two-dimensional isotropic turbulence, Eq. 13 can be written as,

$$E_{22}^{2\mathrm{D}}(k_x) = 2\int_{-\infty}^{\infty} \frac{E^{2\mathrm{D}}}{\pi k}\left(1 - \frac{k_y^2}{k^2}\right)\mathrm{d}k_y. \tag{22}$$

For three-dimensional isotropic turbulence, assuming $k_z = 0$, $E_{22}^{3\mathrm{D}}$ takes the form,

$$E_{22}^{3\mathrm{D}}(k_x, k_z = 0) = 2\int_{-\infty}^{\infty} \frac{E^{3\mathrm{D}}}{4\pi k^2}\left(1 - \frac{k_y^2}{k^2}\right)\mathrm{d}k_y. \tag{23}$$

From Eqs. 22 and 23, it can be inferred that if $E^{2\mathrm{D}}$ follows the shape of $E^{3\mathrm{D}}/(4k)$, the resulting two-dimensional velocity spectra, $\Phi_{22}^{2\mathrm{D}}(k_x, k_y)$, will follow the shape of $\Phi_{22}^{3\mathrm{D}}(k_x, k_y, k_z = 0)$. This can be done by means of the Gaussian superposition technique described in Section V.A.1. The same reasoning applies to the streamwise fluctuating velocity.

Unsteady data collected on the airfoil surface of a two-dimensional CAA simulation are copied repeatedly in the spanwise direction over the full span, $2d$, to generate a three-dimensional airfoil with straight leading edge. The method implies that all panels in the spanwise direction are radiating in phase. By using a three-dimensional FW-H solver the solution is radiated to the far-field under the assumption of uniform mean flow. The configuration is shown in Figure 9.

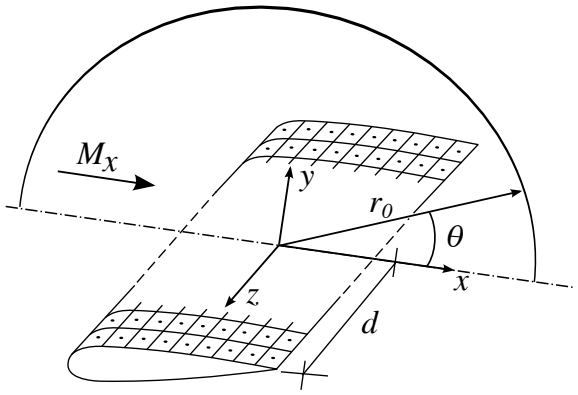

Figure 9. FW-H surface and far-field observer position at the mid-span, d.

The method is validated against Amiet's theory for flat plates in Section V.B.1. Then, the technique is used to reproduce experimental results due to Paterson and Amiet[40] from a NACA 0012 airfoil in Section V.B.2.

V.B.1. Validation Case: Three-dimensional NACA 0001 Airfoil

Amiet's theory[15] is employed to validate the numerical methodology on a 0.15 m chord NACA 0001 airfoil with 0.45 m span, using the advanced digital filter method with pseudo three-dimensional turbulence. The CAA mesh is the same as in Section V.A.2.

For this validation case, $E^{3\mathrm{D}}$ corresponds to the von Kármán energy spectrum, which is defined as,

$$E^{3\mathrm{D}}(k) = \frac{55u_{rms}^2\Lambda}{9\pi}\frac{\left(\frac{k}{k_e}\right)^4}{\left[1 + \left(\frac{k}{k_e}\right)^2\right]^{17/6}}, \tag{24}$$

where $\Lambda = 0.008\,\mathrm{m}$, $T_u = 0.017$ and $k_z = 0$ is assumed.

$N_e = 5$ eddies with the parameters given in Table 3 are required to obtain a good agreement between analytical and numerical results. This is illustrated in Figure 10, where one-dimensional spectra are calculated from fluctuating velocity samples near the airfoil leading edge. The largest disagreement is about 1.5 dB for frequencies above 250 Hz.

It should be noted that when assuming $k_z = 0$ for the turbulence spectra, a π/d scaling factor needs to be applied to all frequencies of the acoustic power spectrum in order to obtain the correct amplitude for the noise predictions.[14] Taking this into account, Figure 11(a) shows PWL and SPL spectra at different observer angles. Since the accuracy of the noise prediction is related to the convergence of the noise spectra, the agreement between analytical and numerical noise levels is also within 1.5 dB.

Λ_i [m]	$u^2_{rms,i}$ [m^2/s^2]
3.618×10^{-2}	4.204×10^{-4}
2.029×10^{-2}	2.149×10^{-3}
1.091×10^{-2}	1.963×10^{-3}
5.524×10^{-3}	1.079×10^{-3}
2.199×10^{-3}	6.760×10^{-4}

Table 3. Parameters for Gaussian superposition in validation case of a NACA 0001 airfoil interacting with pseudo three-dimensional turbulence.

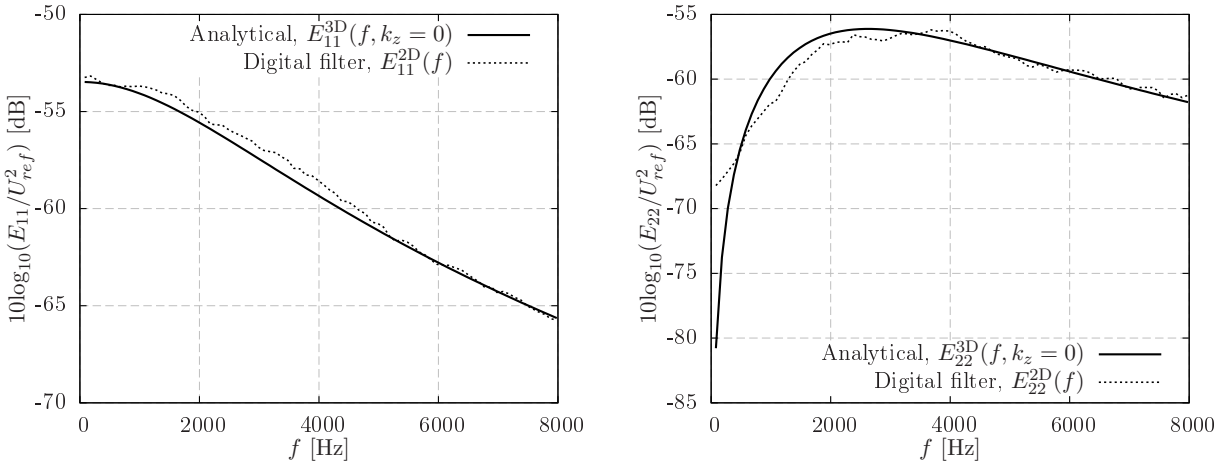

(a) E_{11}^{2D} and E_{11}^{3D}. (b) E_{22}^{2D} and E_{22}^{3D}.

Figure 10. E_{11} and E_{22} spectra for three-dimensional NACA0001 airfoil in a uniform mean flow with $M_x = 0.6$ at approximately $0.02c$ upstream of the airfoil leading edge.

Figure 11(b) shows the directivity pattern at a high frequency, 8000 Hz, in which the shape, position of the lobes and noise levels closely follow those predicted by Amiet's theory[15] at all observer positions in the mid-span plane.

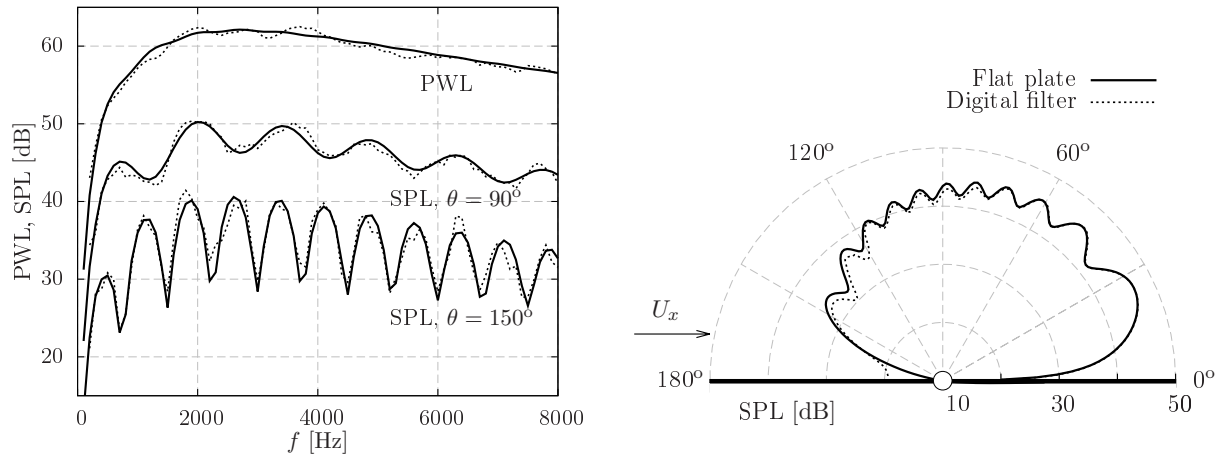

(a) PWL and SPL spectra. (b) Directivity plot at $f = 8000$ Hz.

Figure 11. Far-field noise predictions from a three-dimensional NACA 0001 airfoil at $r_0 = 100c$.

This validation case shows the effectiveness of the methodology proposed herein to realize broadband noise predictions from three-dimensional airfoils with a straight leading edge, by using a coupled approach between two-dimensional CAA simulations and a three-dimensional FW-H solver.

V.B.2. Comparison with Experimental Results from a NACA 0012 Airfoil

Paterson and Amiet[40] performed a series of experiments in an open-jet wind tunnel over a 0.23 m chord NACA 0012 airfoil. In this section, experimental data are compared with numerical results at the speed of 60 m/s, 90 m/s and 120 m/s. For these cases, the turbulence intensities of the transverse component were 3.9%, 4.8% and 4.1%, respectively. The integral length scale was set to approximately 0.03 m for all the cases. The span of the airfoil was $2d = 0.53$ m and the angle of attack was zero. The microphone array was placed outside of the jet shear layer at a distance of $r_0 = 2.25$ m in the mid-span vertical plane.

Experimental measurements were compared with analytical results from a flat plate. The latter were corrected to account for the sound refraction through the shear layer.[15,41] In a similar manner, the same correction is applied to numerical results presented in this section, since the shear layer is not included in the numerical simulation. These are shown in Figure 12, where SPL spectra at $\theta = 90^o$ for the three tunnel speeds are given. Experimental and numerical results are within 2 dB at $U_x = 60$ m/s. However, as the tunnel speed increases, numerical simulations over-predict the experiment. For instance, the largest disagreement is about 4.5 dB at frequencies around 2500 Hz for the 90 m/s case.

It should be noted that for frequencies above 2000 Hz, Paterson and Amiet[40] applied amplitude corrections of up to 4 dB to the experimental data. This was due to the wind tunnel background noise, which caused some uncertainty in the experimental data. Additionally, some necessary inputs for the numerical simulations had to be assumed since these were not specified by Paterson and Amiet.[40] In this sense, the mean flow density was set to 1.2 kg/m^3 for the numerical simulations. A new set of experiments might be required for a better comparison between numerical and experimental results.

An important assumption of the present methodology is that the FW-H solver considers noise propagation in a uniform mean flow before the shear layer correction is applied to the numerical predictions. This implies that potential distortions in the noise radiation around the airfoil are not included. Although SPL spectra at more observers are required to make further conclusions, the shape of the numerical curves follow the trends predicted experimentally.

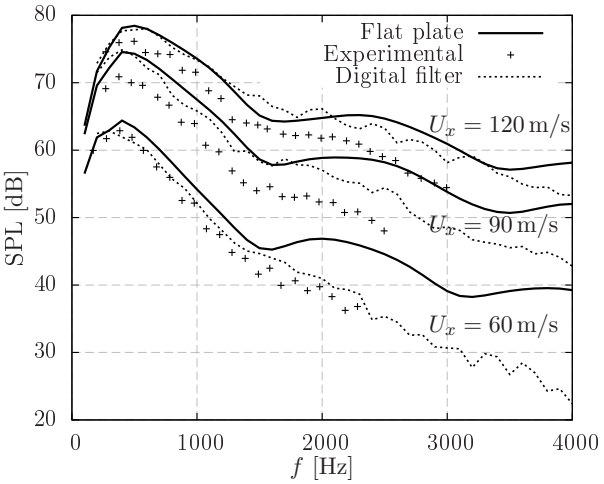

Figure 12. SPL spectra from a NACA 0012 airfoil at $AoA = 0^o$ and observer location $r_0 = 2.25$ m, $\theta = 90^o$.

VI. Comparison with Fourier Mode Methods

The advantages and limitations of the advanced digital filter method to perform leading edge noise predictions are examined herein using purely two-dimensional turbulence. This method is directly compared with the one-component Fourier mode (1cFm) and the two-component Fourier mode (2cFm) approaches presented in Appendix A. A number of isolated airfoil configurations are tested in this section, including variations in mean flow Mach number, airfoil thickness and angle of attack (AoA). A discussion on the computational cost between the different techniques is also included.

All the simulations are performed using the two-dimensional isotropic von Kármán spectrum, where the integral length scale and the turbulence intensity are $\Lambda = 0.008$ m and $T_u = 0.017$, respectively. The chord of the airfoils is set to $c = 0.15$ m.

Fourier mode methods presented in Appendix A produce a turbulent inflow that is repeated in space every $\lambda_{x,max}$. The simulations are run for a transitory state that corresponds to the frozen propagation of the synthetic turbulence over a distance of $\lambda_{x,max}$. Then, each simulation is run for another whole period

of the largest wavenumber involved, while the required unsteady data for the velocity and noise spectra calculation are collected. For the two-component Fourier mode approach, averaging over several realizations is required to obtain converged velocity and noise spectra results. Throughout this work, a total number of 10 independent simulations are used.

Gill *et al.*[10] showed that as the airfoil thickness increases, the noise becomes over-predicted at high frequencies if uniform mean flow is assumed. This is because the turbulent structures are distorted by the non-uniform mean flow, identified as the main source of thick airfoil noise reduction. In addition, viscous mean flows were shown to have little effect on the leading edge noise predictions when compared with inviscid solutions. Consequently, an inviscid non-uniform mean flow is used for the CAA simulations over thick airfoils in this work.

VI.A. Airfoil Thickness and Mach Number Effect on the Noise

NACA 4-series airfoils with 6% and 12% maximum thickness-to-chord ratios are tested at zero angle of attack with free stream Mach numbers $M_x = 0.3$ and $M_x = 0.6$. The values for the Gaussian superposition using the advanced digital filter method and the parameters required for the wavenumber discretization using Fourier mode approaches are given in Appendix B.

For the advanced digital filter method, the inlet section has to be placed upstream enough of the airfoil leading edge to allow for the distortion of the turbulent structures due to the non-uniform mean flow. To investigate this, two different locations are considered for the inlet section in the NACA 0012 airfoil simulations at $M_x = 0.3$ and $M_x = 0.6$. These are $r_{e,1} + c$ and $r_{e,2}$ upstream of the airfoil leading edge, where $r_{e,1} = 5 \max\{\Lambda_i\}/2$ and $r_{e,2} = 3 \max\{\Lambda_i\}/2$, according to the values given in Tables 7 and 8.

A monitor point is placed close to the airfoil leading edge, where one-dimensional spectra are computed. These are presented in Figure 13 for the NACA 0012 airfoil simulations. Results show that both positions of the inlet section lead to similar distortions of the turbulent structures and, consequently, similar noise predictions. E_{11} drops about 3 dB at all frequencies, and the amplitude of E_{22} increases at low frequencies and decreases at high frequencies. A similar behavior was reported by Hunt[42] when analyzing the shape of the velocity spectra around a cylinder by means of the rapid distortion theory developed by Batchelor and Proudman.[43] This implies that, the inlet section can be placed at $r_e \geq 3 \max\{\Lambda_i\}/2$ upstream of the airfoil leading edge in practical cases, even if the mean flow is not completely uniform at this location.

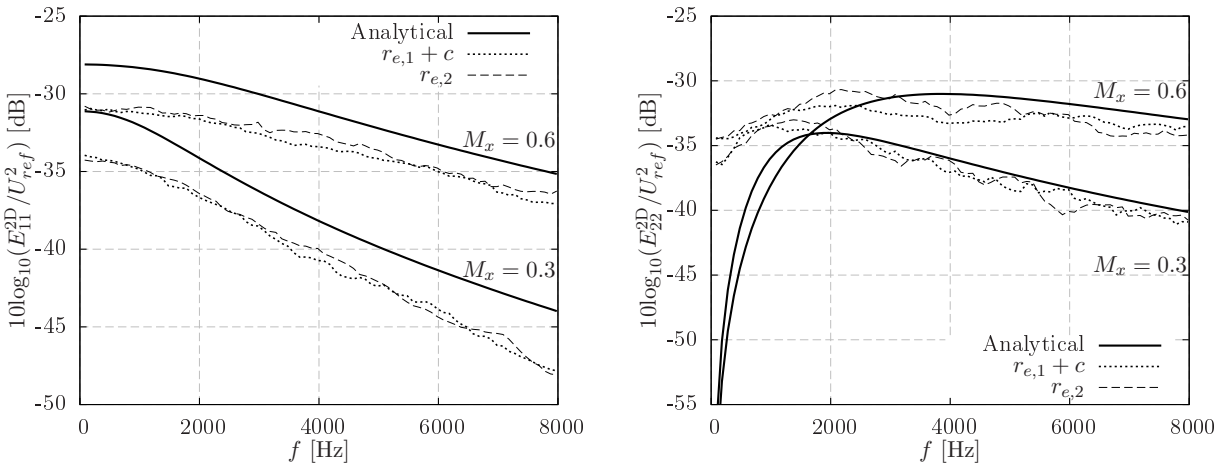

(a) E_{11}^{2D}. (b) E_{22}^{2D}.

Figure 13. One-dimensional spectra at $0.02c$ upstream of the NACA 0012 airfoil leading edge using the advanced digital filter method. The inlet section is placed at two different locations upstream of the airfoil leading edge.

Both E_{11} and E_{22} present a reduction of the amplitude at high frequencies with respect to the prescribed turbulence at the inlet section. Since the distortion of the fluctuating velocity does not happen in the presence of a uniform mean flow, this confirms the over-prediction reported by Gill *et al.*[10] and Clair *et al.*[14]

It is well known that the noise reduction at a fixed acoustic frequency becomes less pronounced at high Mach numbers or small airfoil thickness, as shown by Paterson and Amiet[40] and Gill *et al.*,[10] among others. A similar behavior can also be observed in Figure 14, which plots spectra of PWL. For each of the cases

investigated, all three synthetic turbulence methods predict similar noise levels. Only for the NACA 0012 airfoil simulations, an under-prediction of up to 3 dB is identified at frequencies above 6000 Hz for the one-component Fourier mode approach in comparison with the methods that include two components. This finding, which is not present on the NACA 0006 airfoil simulations, suggests that the fluctuating streamwise component could be necessary for simulations of thick airfoils at high frequencies.[16] Nevertheless, this small disagreement is close to the level of accuracy of the current method (~ 1.5 dB), which makes it difficult to draw further conclusions.

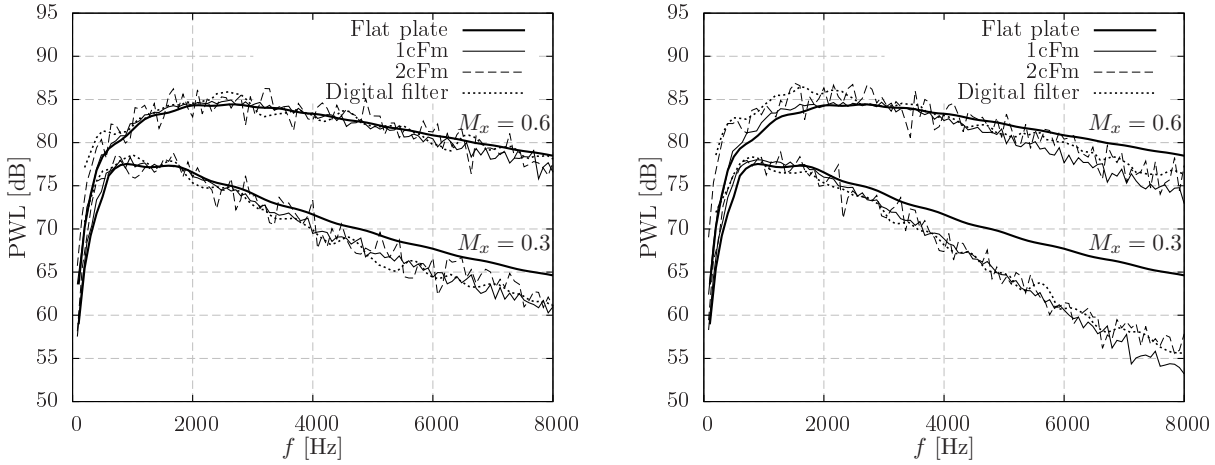

(a) NACA 0006 airfoil.

(b) NACA 0012 airfoil.

Figure 14. PWL spectra at different Mach numbers.

Figure 15 shows fluctuating velocity and pressure contours from all three methods considered in this section. A feature of the advanced digital filter method is that the turbulence can be introduced locally near the airfoil leading edge since each eddy is divergence-free itself. This is not the case for methods based on Fourier modes, in which the turbulence has to be prescribed throughout the CAA domain.

VI.B. Airfoil Angle of Attack Effect on the Noise

In this section, the suitability of the synthetic turbulence methods to study angle of attack is assessed on a NACA 0012 airfoil at $AoA = 6^o$ and $M_x = 0.3$. This configuration was chosen so that a moderate angle of attack can be tested, while the mean flow remains subsonic.

Figure 16 shows PWL predictions from the different techniques. Both the advanced digital filter method and the two-component Fourier mode approach produce noise levels within 2 dB for most frequencies. This is not the case for the one-component Fourier mode approach, which under-predicts the PWL by more than 5 dB for frequencies above 4000 Hz in comparison with synthetic turbulence methods that include two components. Reasons for this under-prediction are discussed in Ref.[16]

The prediction at zero incidence, given by the advanced digital filter method, is included in Figure 16 to highlight the small effect of the angle of attack, as found in previous experimental studies by Moreau *et al.*[44] and Devenport *et al.*,[45] among others.

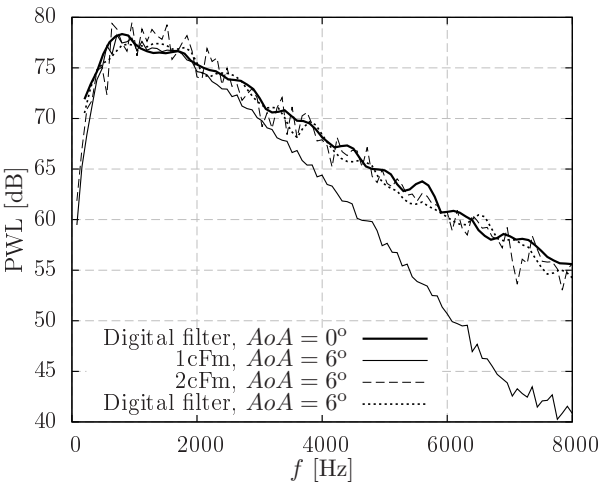

Figure 16. PWL spectra from a NACA 0012 airfoil at $AoA = 6^o$ in a mean flow with $M_x = 0.3$.

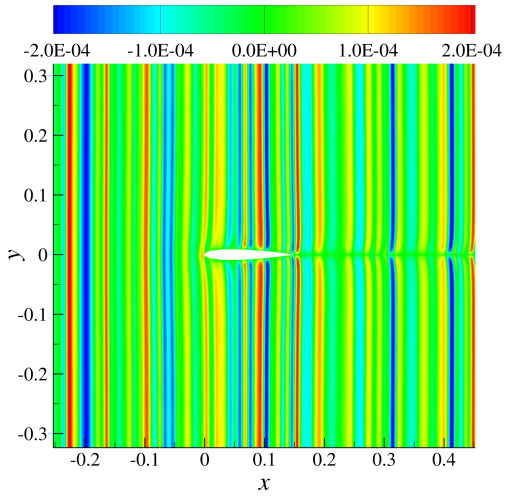

(a) One-component Fourier mode method. Contours of fluctuating velocity, u_y/c_0.

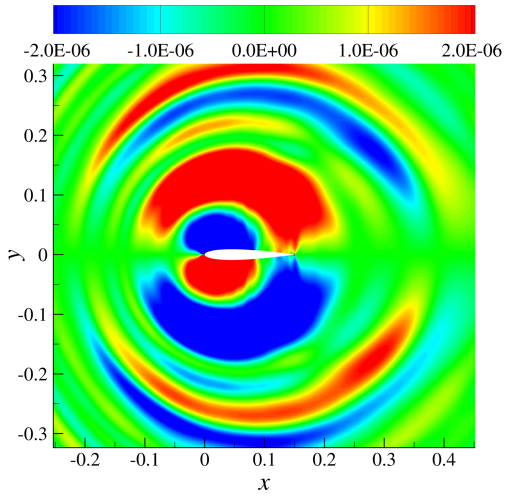

(b) One-component Fourier mode method. Contours of fluctuating pressure, $p/(\rho_0 c_0^2)$.

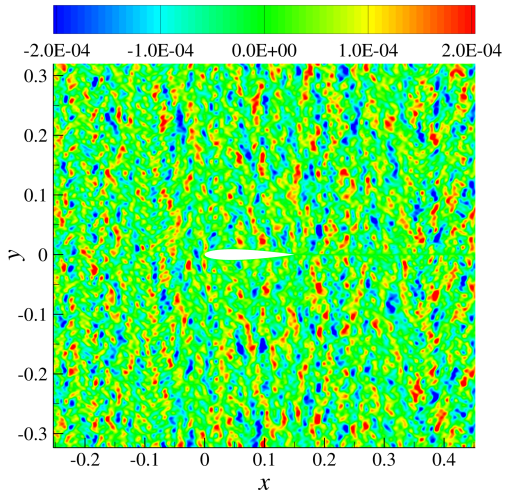

(c) Two-component Fourier mode method. Contours of fluctuating velocity, u_y/c_0.

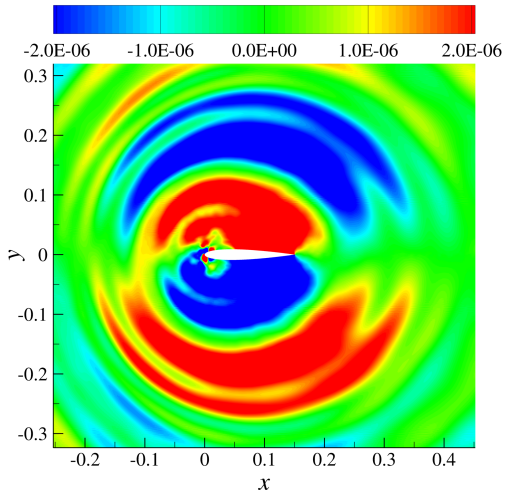

(d) Two-component Fourier mode method. Contours of fluctuating pressure, $p/(\rho_0 c_0^2)$.

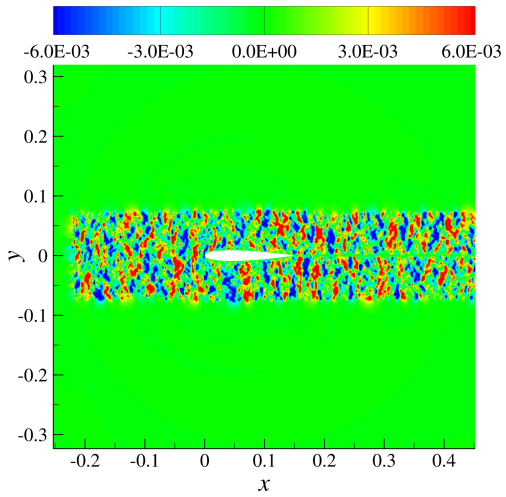

(e) Advanced digital filter method. Contours of fluctuating velocity, u_y/c_0. Inlet section at $r_{e,1} + c$ upstream of the airfoil leading edge.

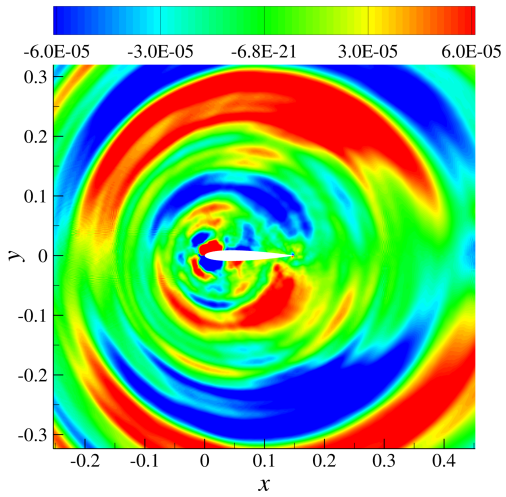

(f) Advanced digital filter method. Contours of fluctuating pressure, $p/(\rho_0 c_0^2)$.

Figure 15. Instantaneous plots of a NACA 0012 airfoil in an inviscid mean flow at $M_x = 0.3$.

VI.C. Computational Cost

A comparison in terms of computational time from the different methods to synthesize turbulence is presented in this section. Since the conclusions of this comparison are similar for all the simulations performed in this paper, only data for the NACA 0012 airfoil at $M_x = 0.3$ and $AoA = 0^o$ are presented. Table 4 shows the computational expense of the different methods. It should be noted that the same CAA mesh and number of processors were used for the simulations of the different synthetic turbulence methods.

The relative comparison shows that the one-component Fourier mode approach is the fastest approach, followed by the advanced digital filter method, which is 4.6 times slower in total. However, a single time step can be run faster with the advanced digital filter method. The difference in the total computational time arises from the total number of time steps that are required to obtain accurate noise predictions. This is due to the fact that only one period of the largest wavelength is necessary to be run for the one-component Fourier mode approach, after the transitory state. The digital filter method, which produces a non-periodic turbulent inflow, has to be run for longer in order for the turbulence and noise spectra to converge.

	Time per time step [s]	No. time steps	Total expense [s]	Expense relative to 1cFm
1cFm	4.541×10^{-2}	84998	3860	1.0
2cFm	8.556×10^{-2}	849980	72721	18.8
Digital filter	4.1765×10^{-2}	424990	17749	4.6

Table 4. Comparison of computational time for a NACA 0012 airfoil at $AoA = 0^o$ and $M_x = 0.3$. The CAA mesh has $821,010$ grid points and 96 cores were used for all the simulations.

The two-component Fourier mode approach is the slowest method among those presented in this work. This is caused by two aspects. Firstly, the total number of Fourier modes in these simulations is $N \times 2M = 2000$, whereas only $N = 100$ modes are required for the one-component Fourier mode method. Secondly, 10 independent realizations are necessary to obtain converged noise results that are within 3 dB accuracy and a transitory state has to be considered for each of them.

From the results presented in Sections VI.A and VI.B, the digital filter method is the best approach among those presented in order to obtain accurate leading edge noise predictions independently of the airfoil thickness, angle of attack and mean flow Mach number at a reasonable computational time. In addition, similar noise predictions can be obtained from both digital filter and Fourier mode methods, provided that both the streamwise and the transverse fluctuating velocity components are included in the simulation.

VII. Three-dimensional Advanced Digital Filter Method

The method presented in Section V.B can only be used in the case of airfoils with straight leading edge. A fully three-dimensional turbulent representation is required when studying more generic cases, such as wavy leading edge airfoils and airfoils with taper or sweep. Among the different approaches presented in Section VI, the advanced digital filter method was found to produce low-cost and accurate noise predictions in all the airfoil configurations that were tested. Therefore, an extension of that method is presented and validated herein to produce three-dimensional isotropic turbulence.

VII.A. Gaussian Energy Spectrum

Following a similar development as described in Section V.A, the three-dimensional energy spectrum function is linked to the spatial filter in wavenumber space through,

$$E^{3D}(k) = 32\pi^4 k^4 \hat{G}(k)^2, \tag{25}$$

where, according to Kraichnan,[11]

$$E^{3D}(k) = \frac{4}{\pi^3} u_{rms}^2 \Lambda^5 k^4 \exp\left(-\frac{\Lambda^2 k^2}{\pi}\right). \tag{26}$$

Thus, the spatial filter in wavenumber space to realize a Gaussian energy spectrum takes the form

$$\hat{G}(k) = \sqrt{\frac{u_{rms}^2 \Lambda^5}{8\pi^7}} \exp\left(-\frac{\Lambda^2 k^2}{2\pi}\right). \tag{27}$$

Taking the inverse Fourier transform of Eq. 27, the spatial filter in physical space reads,

$$G(r) = \sqrt{\frac{u_{rms}^2}{\pi\Lambda}} \exp\left(-\frac{\pi r^2}{2\Lambda^2}\right). \tag{28}$$

When dealing with three velocity components, the RPM method[5] requires the filtering of three statistically independent white-noise signals, $\mathcal{U}_i$ for $i = 1, 2, 3$, whose variances follow,

$$\langle \mathcal{U}_{p,i}^2 \rangle = \int_{V_{s,p}} \langle \mathcal{U}_i(\mathbf{x}', t)\mathcal{U}_i(\mathbf{x}', t) \rangle \, \mathrm{d}\mathbf{x}' = \Delta^3. \tag{29}$$

Therefore, each $\mathcal{U}_{p,i}$ follows a normal distribution $\mathcal{N}(0, \Delta^{3/2})$. The rotational direction of each eddy is now defined by three random numbers ϵ_x, ϵ_y and ϵ_z, which can independently be $+1$ or -1.

The three-dimensional velocity field introduced by each Gaussian eddy takes the form,

$$u_x(\mathbf{x}) = \frac{\Delta^{3/2} u_{rms}}{\Lambda^2} \sqrt{\frac{\pi}{\Lambda}} \left[\epsilon_y (z - z_e) - \epsilon_z (y - y_e)\right] \exp\left(-\frac{\pi r^2}{2\Lambda^2}\right), \tag{30}$$

$$u_y(\mathbf{x}) = \frac{\Delta^{3/2} u_{rms}}{\Lambda^2} \sqrt{\frac{\pi}{\Lambda}} \left[\epsilon_z (x - x_e) - \epsilon_x (z - z_e)\right] \exp\left(-\frac{\pi r^2}{2\Lambda^2}\right), \tag{31}$$

$$u_z(\mathbf{x}) = \frac{\Delta^{3/2} u_{rms}}{\Lambda^2} \sqrt{\frac{\pi}{\Lambda}} \left[\epsilon_x (y - y_e) - \epsilon_y (x - x_e)\right] \exp\left(-\frac{\pi r^2}{2\Lambda^2}\right). \tag{32}$$

Figure 17(a) shows contours of fluctuating velocity magnitude from isolated eddies using Eqs. 30, 31 and 32. A number of these eddies can be combined to realize three-dimensional isotropic turbulence following a similar inlet section approach as for two-dimensional cases (see Section V.A). An instantaneous plot of synthetic turbulence is depicted in Figure 17(b).

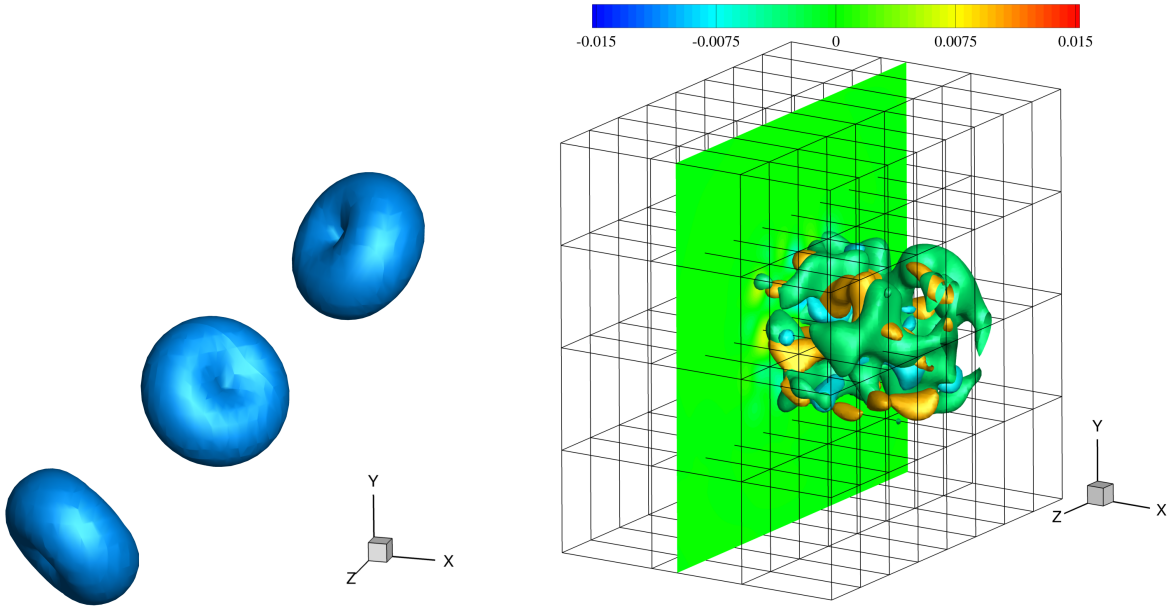

(a) Three-dimensional eddies. Contours of fluctuating velocity magnitude.

(b) Three-dimensional turbulence. Iso-contours of velocity fluctuations, $u_x/c_0 = 0.01$, $u_y/c_0 = -0.005$ and $u_z/c_0 = -0.01$. The mean flow velocity is set to $U_x = 60\,\mathrm{m/s}$ and the turbulence intensity and integral length scale are, $T_u = 0.017$ and $\Lambda = 0.008\,\mathrm{m}$, respectively.

Figure 17. Instantaneous plots of three-dimensional eddies and synthetic turbulence.

It can be shown that the normalized diameter of each three-dimensional eddy, $2r_{e,max}/\Lambda$, is approximately the same as a two-dimensional eddy defined by Eqs. 10 and 11. Therefore, the limiting values discussed in Section V.A remain valid, and one-dimensional spectra are realized providing that $r_e \geq 3\Lambda/2$ and $\Delta \leq \Lambda/2$. This is shown in Figure 18, where numerical results are in good agreement with the analytical expressions.

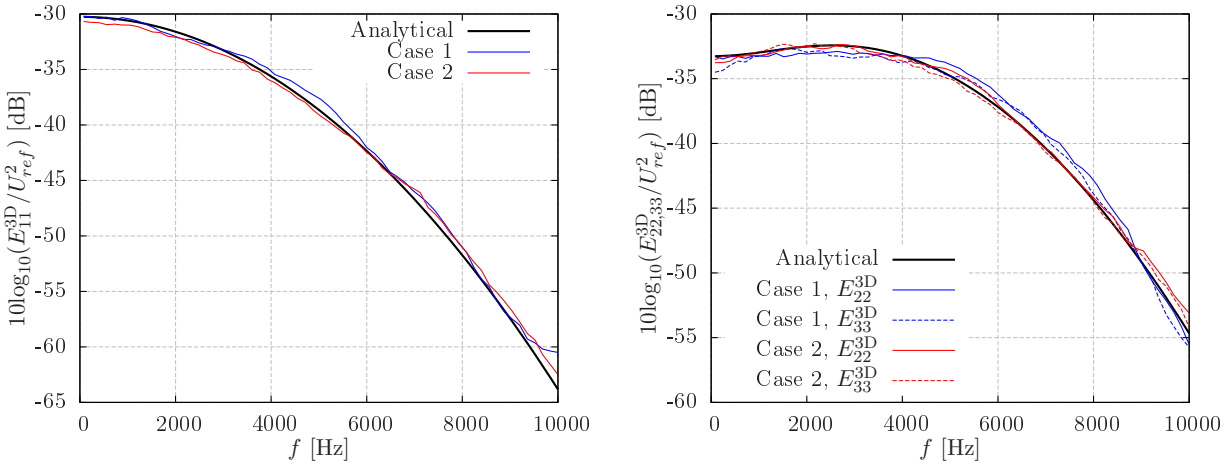

(a) E_{11}^{3D}. (b) E_{22}^{3D} and E_{33}^{3D}.

Figure 18. One-dimensional Gaussian spectra. Case 1 corresponds to $\Delta = \Lambda/2$ and $r_e = 3\Lambda/2$ and Case 2 corresponds to $\Delta = \Lambda/6$ and $r_e = 5\Lambda/2$.

VII.B. Non-Gaussian Energy Spectra Through Gaussian Superposition

As proposed in Section V.A.1, a desired three-dimensional energy spectrum can be achieved by defining a new eddy shape from the superposition of several Gaussian eddies. Using Eq. 25, the target energy spectrum takes the form,

$$E_{sum}^{3D}(k) = 32\pi^4 k^4 \left[\sum_{i=1}^{N_e} \hat{G}_i(\Lambda_i, u_{rms,i}^2, k)\right]^2 . \tag{33}$$

Introducing Eq. 27 into Eq. 33, the resulting energy spectrum from the Gaussian superposition reads

$$E_{sum}^{3D}(k) = \frac{4k^4}{\pi^3} \sum_{i=1}^{N_e}\sum_{j=1}^{N_e} \sqrt{u_{rms,i}^2 u_{rms,j}^2 \Lambda_i^5 \Lambda_j^5} \exp\left[-\frac{k^2}{2\pi}\left(\Lambda_i^2 + \Lambda_j^2\right)\right] . \tag{34}$$

VIII. Conclusions

An advanced digital filter method to generate synthetic turbulence is presented in this work. The technique consists of a simple and fast implementation of the RPM[5,6] method that adopts some ideas from synthetic eddy methods.[25,26,27] Discretized equations for the velocity field defined by each eddy are given to realize a desired isotropic energy spectrum through a superposition of Gaussian spectra. These are directly introduced into the CAA domain through an inlet section without requiring any special boundary conditions.

The governing equations are derived and validated to realize purely two-dimensional turbulence. A low-cost methodology is also presented to realize a two-dimensional turbulent flow that follows the governing equations of three-dimensional turbulence. To this end, the spanwise wavenumber component is set to zero, $k_z = 0$, according to Amiet's theory.[15] The technique combines two-dimensional CAA simulations using the advanced digital filter with a three-dimensional FW-H solver for the far-field propagation. This approach is successfully used to reproduce experimental measurements from a NACA 0012 airfoil with straight leading edge.[40] In particular, numerical noise predictions follow the same behavior as found experimentally and the agreement is within 3 dB for the majority of the tested tunnel speeds and frequencies. This shows that three-dimensional CAA simulations are not necessary to obtain accurate noise predictions that can be compared with experimental results.

Leading edge noise predictions from the advanced digital filter method are also compared to those provided by one- and two-component Fourier mode approaches. Numerical results show that the one-component Fourier mode approach, which is the simplest and fastest synthetic turbulence method of those tested, produces satisfactory noise predictions for symmetric airfoils with moderate thickness at zero angle of attack.

However, either the advanced digital filter method or the two-component Fourier mode approach is required when considering thick airfoils and non-zero angle of attack. Additionally, it is shown that turbulence-airfoil interaction noise using the LEEs is independent of the synthetic turbulence method, provided that both the transverse and the streamwise components are included. Two-dimensional simulations using the advanced digital filter method are about four times faster and present a better convergence in terms of turbulence and noise spectra. One can conclude that the advanced digital filter method is the most versatile approach among those analyzed for leading edge noise predictions.

In addition, simulations using the advanced digital filter method show the same behavior that was reported in experiments to measure turbulence-airfoil interaction noise.[40,44,45] It is assessed that the airfoil thickness decreases the noise radiated at high frequencies, especially at low Mach numbers, and the angle of attack has little effect on the noise levels. Furthermore, the over-prediction at high frequencies from CAA simulations assuming uniform mean flow[10,14] is associated to the fact that the incoming turbulence is not distorted in the vicinity of the stagnation region.

Two-dimensional CAA simulations cannot be used when studying more generic cases, such as wavy leading edge airfoils. In this case, the spanwise wavenumber and fluctuating velocity might not be negligible for accurate turbulence-airfoil interaction noise predictions. Thus, the governing equations to realize fully three-dimensional synthetic turbulence are derived.

Acknowledgements

The research funding for this project was partially provided by the University of Southampton and Innovate UK (Technology Strategy Board), as part of the wHole AiRcraft Multidisciplinary nOise desigN sYstem (HARMONY) program.

Appendices

A. Methods based on a Summation of Fourier Modes

Two different approaches to generate two-dimensional synthetic turbulence based on Fourier modes are considered in this appendix. A one-component Fourier mode approach is first presented in Section A.A. In this case, only the transverse fluctuating velocity is modeled. In Section A.B, both the transverse and the streamwise velocity disturbances are used to describe the incoming turbulence, which provides a more realistic definition of the turbulent flow. The governing equations of these methods are based on previous works by Béchara *et al.*[12] and Bailly and Juvé,[13] among others.

A.A. One-component Fourier Mode (1cFm) Summation

In this case, the fluctuating velocity field can be seen as a superposition of plane waves, whose amplitude is modulated by the velocity spectrum of the transverse disturbances. The fluctuating velocity field can be written as,

$$u_y(\mathbf{x},t) = \sum_{n=1}^{N} \sqrt{\Phi_{22}^{2\mathrm{D}}\left(k_{x,n}\right)\Delta k_{x,n}}\cos\left[k_{x,n}\left(x-U_x t\right)+\phi_n\right], \tag{35}$$

where N is the total number of modes, U_x is the mean flow velocity, ϕ_n is the random phase term, $k_{x,n}$ is the streamwise wavenumber component and $\Delta k_{x,n}$ is related to the wavenumber discretization. The velocity spectrum to be used in Eq. 35 is obtained after integration over the transverse wavenumber component,

$$\Phi_{22}^{2\mathrm{D}}\left(k_x\right) = \int_{-\infty}^{+\infty} \Phi_{22}^{2\mathrm{D}}\left(k_x,k_y\right)\mathrm{d}k_y, \tag{36}$$

where the velocity spectrum of the i^{th} turbulent velocity component is linked to the energy spectrum by

$$\Phi_{ii}^{2\mathrm{D}}\left(k_x,k_y\right) = \frac{E^{2\mathrm{D}}(k)}{\pi k}\left(1-\frac{k_i^2}{k^2}\right). \tag{37}$$

The streamwise wavenumber discretization follows a uniform distribution with a constant Δk_x. Since $k_x = 2\pi/\lambda_x$, Fourier modes are selected so that their wavelengths are: $\lambda_{x,max}$, $\lambda_{x,max}/2$, $\lambda_{x,max}/3$, ..., $\lambda_{x,max}/N$. Thus, the incoming turbulence has a finite number of discrete frequencies, N, and is periodic with a period related to the largest wavelength $\lambda_{x,max}$.

Although different approaches exist to implement a turbulent inflow using Fourier modes, all of them focus on introducing the fluctuating velocity without producing spurious noise. For instance, Clair *et al.*[14] used a turbulent inflow based on Tam's boundary conditions.[46] In this work, the synthetic turbulence is defined within the buffer zones, where the mean flow is required to be uniform, as stated by Eq. 35. Otherwise, spurious sources of noise may appear at the buffer zone exit. In order to reduce the computational time, the fluctuating velocity field is initialized throughout the CAA domain at the beginning of the simulation, which helps to reduce the expense of the transitory state.

A.B. Two-component Fourier Mode (2cFm) Summation

The two-component turbulent inflow provides a more realistic definition of the vortical perturbations. It is defined as follows,

$$\mathbf{u}(\mathbf{x},t) = \sum_{n=1}^{N}\sum_{m=1}^{2M}\sqrt{E^{2\mathrm{D}}(k)\,\frac{\Delta k_{x,n}\Delta k_{y,m}}{\pi k}}\cos\left[k_{x,n}\left(x-U_x t\right)+k_{y,m}y+\phi_{nm}\right]\boldsymbol{\sigma}_{nm}, \tag{38}$$

where ϕ_{nm} is the random phase term, $k = \sqrt{k_{x,n}^2 + k_{y,m}^2}$ is the overall wavenumber, $\Delta k_{x,n}$ and $\Delta k_{y,m}$ are related to the wavenumber discretization and $\boldsymbol{\sigma}_{nm}$ is a unit vector ($\|\boldsymbol{\sigma}_{nm}\| = 1$) that guarantees the divergence-free condition ($\boldsymbol{\sigma}_{nm}\cdot\mathbf{k} = 0$). Thus, for a purely two-dimensional flow field realization $\sigma_{x,nm} = \pm k_{y,m}/k$ and $\sigma_{y,nm} = \mp k_{x,n}/k$.

The $k_{x,m}$ discretization follows the uniform distribution proposed in Section A.A. The $k_{y,m}$ discretization is performed so that there is the same number of positive and negative $k_{y,m}$. In order to obtain a good representation of the spectral content while minimizing the number of modes in the transverse direction, a logarithmic distribution is adopted in this case. Following Béchara *et al.*'s[12] work, the M positive $k_{y,m}$ are defined as

$$k_{y,m} = \exp\left[\log_{\mathrm{e}}(k_{y,min}) + (m - M - 1)\Delta k_y'\right], \tag{39}$$

where $m = M+1, ..., 2M$ and the auxiliary term $\Delta k_y'$ is defined as

$$\Delta k_y' = \frac{\log_{\mathrm{e}}(k_{y,max}) - \log_{\mathrm{e}}(k_{y,min})}{M-1}. \tag{40}$$

In practice, $k_{y,min} = k_{x,min} > 0$ and $k_{y,max} = C k_{x,max} > 0$, where C usually takes a value between 2 and 3, depending on the energy spectrum to be matched. Unlike the $\Delta k_{x,n}$ term, the $\Delta k_{y,m}$ distribution is not constant. In the present work, it is approximated as $\Delta k_{y,m} = (k_{y,m-1} - k_{y,m+1})/2$ if $m = 2, ..., 2M-1$, $\Delta k_{y,m=1} = \Delta k_{y,m=2}$ and $\Delta k_{y,m=2M} = \Delta k_{y,m=2M-1}$. The M negative $k_{y,m}$ modes are repeated symmetrically so that $k_{y,m=1} = -k_{y,m=2M}, ..., k_{y,m=M} = -k_{y,m=M+1}$.

B. Input Parameters for Two-dimensional Leading Edge Noise Predictions

In this appendix, the input values for the synthetic turbulence methods used in Section VI are detailed. Note that these values are used to realize a two-dimensional von Kármán spectrum with $\Lambda = 0.008\,\mathrm{m}$ and $T_u = 0.017$.

	$\lambda_{x,max}$ [m]	N	M	C
1cFm	1.275	100	–	–
2cFm	1.275	100	10	2

Table 5. Parameters for one- and two-component Fourier mode methods. The mean flow Mach number is $M_x = 0.3$.

	$\lambda_{x,max}$ [m]	N	M	C
1cFm	2.55	100	–	–
2cFm	2.55	100	10	3

Table 6. Parameters for one- and two-component Fourier mode methods. The mean flow Mach number is $M_x = 0.6$.

The input parameters for the one- and two-component Fourier mode approaches at $M_x = 0.3$ and $M_x = 0.6$ are given in Tables 5 and 6, respectively. The integral length scale and the root-mean-square of the velocity fluctuations for Gaussian superposition in the advanced digital filter method are given in Tables 7 and 8.

Λ_i [m]	$u^2_{rms,i}$ [m^2/s^2]
2.524×10^{-2}	5.194×10^{-2}
1.401×10^{-2}	2.152×10^{-1}
7.285×10^{-3}	3.012×10^{-1}
3.023×10^{-3}	4.667×10^{-1}
2.238×10^{-3}	8.929×10^{-3}

Table 7. Parameters for Gaussian superposition using the advanced digital filter method. The mean flow Mach number is $M_x = 0.3$.

Λ_i [m]	$u^2_{rms,i}$ [m^2/s^2]
2.524×10^{-2}	2.077×10^{-1}
1.401×10^{-2}	8.608×10^{-1}
7.285×10^{-3}	1.205
3.023×10^{-3}	1.867
2.238×10^{-3}	3.566×10^{-2}

Table 8. Parameters for Gaussian superposition using the advanced digital filter method. The mean flow Mach number is $M_x = 0.6$.

References

[1] "Global Market Forecast. Future Journeys 2013-2032," *Full book from www.airbus.com*, Airbus, 2013.

[2] "Aeronautics and Air Transport Beyond Vision 2020 (Towards 2050)," *The Advisory Council for Aeronautics Research in Europe*, 2010.

[3] Astley, R. J., Agarwal, A., Holland, K. R., Joseph, P. F., Self, R. H., Smith, M. G., Sugimoto, R., Tester, B. J., "Predicting and Reducing Aircraft Noise," *14th International Congress on Sound and Vibration*, Australia, 2007.

[4] Ganz, U. W., Joppa, P. D., Patten, T. J., Scharpf, D. F, "Boeing 18-Inch Fan Rig Broadband Noise Test," *NASA Contractor Report*, CR-1998-208704, 1998.

[5] Ewert, R., "Broadband Slat Noise Prediction based on CAA and Stochastic Sound Sources from a Fast Random Particle-Mesh (RPM) Method," *Journal of Computers and Fluids*, Vol. 37, pp. 369-387, 2008.

[6] Dieste, M., Gabard, G., "Random Particle Methods Applied to Broadband Fan Interaction Noise," *Journal of Computational Physics*, Vol. 231, No. 24, pp. 8133-8151, 2012.

[7] Sandberg, R. D., Jones, L. E., "Direct Numerical Simulations of Airfoil Self-Noise," *IUTAM Symposium on Computational Aero-Acoustics for Aircraft Noise Prediction*, Procedia Engineering, Vol. 6, pp. 274-282, 2010.

[8] Atassi, H., M., Subramaniam, S., Scott, J. R., "Acoustic Radiation from Lifting Airfoils in Compressible Subsonic Flow," *NASA Technical Memorandum*, No. 103650, 1990.

[9] Lockard, D. P., Morris, P. J., "Radiated Noise from Airfoils in Realistic Mean Flows," *AIAA Journal*, Vol. 36, No. 6, pp. 907-914, 1998.

[10] Gill, J., Zhang, X., Joseph, P., "Symmetric Airfoil Geometry Effects on Leading Edge Noise," *Journal of the Acoustical Society of America*, Vol. 134, No. 4, pp. 2669-2680, 2013.

[11] Kraichnan, R. H., "Diffusion by a Random Velocity Field," *The Physics of Fluids*, Vol. 13, No. 1, pp. 22-31, 1970.

[12] Béchara, W., Bailly, C., Lafon, P., Candel, S. M., "Stochastic Approach to Noise Modeling for Free Turbulent Flows," *AIAA Journal*, Vol. 32, No. 3, pp. 455-463, 1994.

[13] Bailly, C., Juvé, D., "A Stochastic Approach to Compute Subsonic Noise using Linearized Euler's Equations," *5th AIAA/CEAS Aeroacoustics Conference*, No. AIAA 99-1872, 1999.

[14] Clair, V., Polacsek, C., Le Garrec, T., Reboul, G., Gruber, M., Joseph, P. "Experimental and Numerical Investigation of Turbulence-Airfoil Noise Reduction using Wavy Edges," *AIAA Journal*, Vol. 51, No. 11, pp. 2695-2713, 2013.

[15] Amiet, R. K., "Acoustic Radiation from an Airfoil in a Turbulent Stream", *Journal of Sound and Vibration*, Vol. 41, No. 4, pp. 407-420, 1975.

[16] Gill, J., "Broadband Noise Generation of a Contra-Rotating Open Rotor Blade," *Thesis for the degree of Doctor of Engineering, Airbus Noise Technology Centre, University of Southampton*, 2015.

[17] Ewert, R., Appel, C., Dierke, J., Herr, M., "RANS/CAA based Prediction of NACA 0012 Broadband Trailing Edge Noise and Experimental Validation," *15th AIAA/CEAS Aeroacoustics Conference*, No. AIAA 2009-3269, 2009.

[18] Siefert, M., Ewert, R., "Sweeping Sound Generation in Jets Realized with a Random Particle-Mesh Method," *15th AIAA/CEAS Aeroacoustics Conference*, No. AIAA 2009-3369, 2009.

[19] Wohlbrandt, A. M., Gurin, S., Ewert, R., "Simultaneous Computation of Surface and Volume Sources for Fan Broadband Noise with the Random-Particle-Mesh Method," *19th AIAA/CEAS Aeroacoustics Conference*, No. AIAA 2013-2119, 2013.

[20] Ewert, R., "Acoustic Perturbation Equations based on Flow Decomposition via Source Filtering," *Journal of Computational Physics*, Vol. 188, No. 2, pp. 365-398, 2003.

[21] Kim, D., Heo, S., Cheong, C., "Time-domain Inflow Boundary Condition for Turbulence-airfoil Interaction Noise Prediction using Synthetic Turbulence Modeling," *Journal of Sound and Vibration*, Vol. 340, pp. 138-151, 2015.

[22] Tam, C. K. W., Dong, Z., "Radiation and Outflow Boundary Conditions for Direct Computation of Acoustic and Flow Disturbances in a Nonuniform Mean Flow," *Journal of Computational Acoustics*, Vol. 4, No. 2, pp. 157-201, 1996.

[23] Giles, M., "Nonreflecting Boundary Conditions for Euler Equation Calculations," *AIAA Journal*, Vol. 28, No. 12, pp. 2050-2058, 1990.

[24] Kim, D., Lee, G-S., Cheong, C., "Inflow Broadband Noise From an Isolated Symmetric Airfoil Interacting with Incident Turbulence," *Journal of Fluids and Structures*, Vol. 55, pp. 428-450, 2015.

[25] Jarrin, N., Benhamadouche, S., Laurence, D., Prosser, R., "A Synthetic-Eddy-Method for generating Inflow Conditions for Large-Eddy Simulations," *International Journal of Heat and Fluid Flow*, Vol. 27, pp. 585-593, 2006.

[26] Sescu, A., Hixon, R., "Towards Low-Noise Synthetic Turbulent Inflow Conditions for Aeroacoustic Calculations," *International Journal for Numerical Methods in Fluids*, Vol. 73, pp. 1001-1010, 2013.

[27]Kim, J. W., Haeri, S., "An Advanced Synthetic Eddy Method for the Computation of Aerofoil-Turbulence Interaction Noise," *Journal of Computational Physics*, Vol. 287, pp. 1-17, 2015.

[28]Zhang, X., Chen, X. X., and Nelson, P. A., "Computation of Spinning Modal Radiation from an Unflanged Duct," *AIAA Journal*, Vol. 42, No. 6, pp. 1795-1801, 2004.

[29]Wang, X., Hu, Z., Zhang, X., "Aeroacoustic Effects of High-lift Wing Slat Track and Cut-out System," *International Journal of Aeroacoustics*, Vol. 12, No. 3, pp. 283-308, 2013.

[30]Liu, W., Kim, J. W., Zhang, X., Angland, D., Bastien, C., "Landing Gear Noise Prediction using High-order Finite Difference Schemes," *Journal of Sound and Vibration*, Vol. 332, No. 14, pp. 3517-3534, 2013.

[31]Kim, J. W., "Optimised Boundary Compact Finite Difference Schemes for Computational Aeroacoustics," *Journal of Computational Physics*, Vol. 225, No. 1, pp. 995-1019, 2007.

[32]Kim, J. W., "High-Order Compact Filters with Variable Cut-Off Wavenumber and Stable Boundary Treatment," *Journal of Computers and Fluids*, Vol. 39, No. 7, pp. 1168-1182, 2010.

[33]Hu, F. Q., Hussaini, M. Y., Manthey, J., "Low-Dissipation and -Dispersion Runge-Kutta Schemes for Computational Acoustics," *Journal of Computational Physics*, Vol. 124, pp. 177-191, 1996.

[34]Gill, J., Fattah, R., Zhang, X., "Optimization of Non-Reflective Boundary Conditions for Aeroacoustic Simulations," *21st AIAA/CEAS Aeroacoustics Conference*, 2015.

[35]Taylor, G. I., "The Spectrum of Turbulence," *Proceedings of the Royal Society of London, Series A, Mathematical and Physical Sciences*, Vol. 164, No. 919, pp. 476-490, 1938.

[36]Pope, S. B., "Turbulent Flows," *Cambridge University Press*, 2000.

[37]Dieste, M., "Random-Vortex-Particle Methods Applied to Broadband Fan Interaction Noise," *Thesis for the degree of Doctor of Philosophy, ISVR, University of Southampton*, 2011.

[38]Blandeau, V.P., Joseph, P. F., Jenkins, G., Powles, C. J, "Comparison of Sound Power Radiation from Isolated Airfoils and Cascades in a Turbulent Flow," *Journal of the Acoustical Society of America*, Vol. 129, No. 6, pp. 3521-3530, 2011.

[39]Farassat, F., Succi, G. P., "The Prediction of Helicopter Discrete Frequency Noise," *Vertica*, Vol. 7, No. 4, pp. 309-320, 1983.

[40]Paterson, R. W., Amiet, R. K., "Acoustic Radiation and Surface Pressure Characteristics of an Airfoil due to Incident Turbulence," *NASA Contractor Report*, CR-2733, 1976.

[41]Amiet, R. K., "Correction of Open Jet Wind Tunnel Measurements for Shear Layer Refraction," *2nd AIAA Aeroacoustics Conference*, No. AIAA 75-532, 1975.

[42]Hunt, J. C. R., "A Theory of Turbulent Flow Round Two-dimensional Bluff Bodies," *Journal of Fluid Mechanics*, Vol. 61, Part. 4, pp. 625-706, 1973.

[43]Batchelor, G. K., Proudman, I., "The Effect of Rapid Distortion of a Fluid in Turbulent Motion," *Quarterly Journal of Mechanics and Applied Mathematics*, Vol. 7, No. 1, pp. 83-103, 1954.

[44]Moreau, S., Roger, M., Jurdic, V., "Effect of Angle of Attack and Airfoil Shape on Turbulence-Interaction Noise," *11th AIAA/CEAS Aeroacoustics Conference*, No. AIAA 2005-2973, 2005.

[45]Devenport, W. J., Staubs, J. K., Glegg, S. A. L., "Sound Radiation from Real Airfoils in Turbulence," *Journal of Sound and Vibration*, Vol. 329, pp. 3470-3483, 2010.

[46]Tam, C. K. W., "Advances in Numerical Boundary Conditions for Computational Aeroacoustics," *13th Computational Fluid Dynamics Conference*, No. 1774, 1997.